École polytechnique de Louvain

Spectral efficiency and EMF exposure in cellular and cell-free massive MIMO networks : a comparative analysis

Author: **Julien Giunta**
Supervisors: **Claude Oestges, Luc Vandendorpe**
Readers: **Charles Wiame, Jérôme Louveaux**
Academic year 2023–2024
Master [120] in Electrical Engineering

Abstract

In an era where Quality of Service (QoS) demands are on the rise, the increasing number of connected devices highlights the need for more consistent coverage. The growth in connectivity needs is particularly evident with the widespread use of Internet of Things (IoT) devices. Cell-free networks appear to be a promising solution to meet the growing demand for seamless and reliable communication. However, despite their potential advantages, these innovative networks raise concerns, especially regarding potential health risks linked to EMF exposure. This master thesis focuses on comparing cell-free networks with existing cellular networks, assessing their spectral efficiency and exposure to EMF through numerical simulations. Both of these crucial aspects are examined using various statistical metrics for a comprehensive evaluation. The system models used to simulate these networks are carefully defined, aiming to ensure consistency. However, some limitations associated with comparing these two types of networks are also discussed to ensure an informed interpretation of the obtained results.

***Index Terms*–Cell-free networks, Cellular networks, mMIMO, Spectral efficiency, EMF exposure**

Contents

Acronyms

3GPP	3rd generation partnership project
AP	Access point
BS	Base station
CCDF	Complementary cumulative distribution function
CF	Cell-free
CPU	Central processing unit
CSI	Channel state information
DCC	Dynamic cooperation clustering
EMF	Electromagnetic field
ICNIRP	International commission on non-ionizing radiation protection
IPD	Incident power density
M-MMSE	Multicell minimum mean squared error
MIMO	Multiple input multiple output
mMIMO	Massive MIMO
MMSE	Minimum mean squared error
MR	Maximum ratio
MSE	Mean-squared error
NLoS	Non line-of-sight

P-MMSE	Partial minimum mean squared error
P-RZF	Partial regularized zero forcing
RF	Radio frequency
RRH	Remote radio head
RZF	Regularized zero forcing
S-MMSE	Single-cell minimum mean squared error
SAR	Specific absorption rate
SDMA	Space-division multiple access
SE	Spectral efficiency
SINR	Signal-to-interference-plus-noise-ratio
TDD	Time-division duplex
UE	User equipment

List of Symbols

Cellular

β_{lk}^{j}	The large-scale fading coefficient model of the channel between the BS j and the UE k in cell l
$\mathbf{C}_{jk}^{l}$	The error correlation matrix of the channel between UE k in cell j and BS l
F_{lk}^{j}	Shadow fading coefficient of the channel between BS j and UE k in cell l
$\mathbf{h}_{lk}^{j}$	The channel vector between BS j and UE k in cell l. $\mathbf{h}_{lk}^{j} \in \mathbb{C}^{N_j}$
$\widehat{\mathbf{h}}_{lk}^{j}$	The MMSE estimate of $\mathbf{h}_{kl}^{j}$
K_j	The number UEs per cell (the same in each cell)
L	The number of BSs/cells in the network
N_j	The number of antennas per BS
$\mathcal{P}_{jk}$	The set of indices of UEs sharing the same pilot sequence as UE k in cell j, including itself
$\boldsymbol{\phi}_{jk}$	The pilot sequence allocated to UE k in cell j
$\mathbf{R}_{lk}^{j}$	Spatial correlation matrix of channel $\mathbf{h}_{lk}^{j}$
t_{jk}	The pilot index of UE k in cell j
$\mathbf{w}_{jk}$	The unit-norm precoding vector assigned by BS j to UE k in cell j
$\mathbf{x}_l$	The downlink transmitted data signal by BS l
ξ_{jk}	EMF exposure experienced by UE k in cell j
y_{jk}^{dl}	The received downlink signal at UE k in cell j

Cell-free

β_{kl}	The large-scale fading coefficient model of the channel between the AP l and the UE k
$\mathbf{C}_{kl}$	The error correlation matrix of the channel between UE k and AP l

$\mathbf{D}_{kl}$	The set of diagonal matrices $\mathbf{D}_{kl} \in \mathbb{C}^{N\times N}$ determining which APs communicate with which UEs
$\mathcal{D}_l$	The set of UEs served by AP l
F_{kl}	Shadow fading coefficient of the channel between AP l and UE k
$\mathbf{h}_{kl}$	The channel vector between AP l and UE k in an arbitrary coherence block
$\widehat{\mathbf{h}}_{kl}$	The MMSE estimate of $\mathbf{h}_{kl}$
L	The number of APs in the network
K	The number of UEs in the network
$\mathcal{M}_k$	The subset of AP's indices serving the user UE k
N	The number of antennas per AP
$\boldsymbol{\phi}_k$	The pilot sequence of UE k
ς_{jk}	The data signal assigned to UE k in cell j
$\mathcal{P}_k$	The set of indices of UEs sharing the same pilot sequence as UE k, including itself
$\mathbf{R}_{kl}$	Spatial correlation matrix of channel $\mathbf{h}_{kl}$
ς_k	The data signal assigned to UE k
t_k	The pilot index of UE k
$\mathbf{w}_{kl}$	The transmit precoding vector $\mathbf{w}_{kl} \in \mathbb{C}^N$ that AP l assigns to UE k
ξ_k	EMF exposure experienced by UE k
$\mathbf{x}_l$	The downlink transmitted data signal by AP l
y_k^{dl}	The received downlink signal at UE k

Global

$\mathbf{0}_{N\times M}$	The $N \times M$ matrix with only zeros
B_c	The coherence bandwidth of the systems
c	Speed of light in vacuum
$\mathbb{C}^{N\times M}$	The set of complex-valued $N \times M$ matrices
$\mathbf{I}_N$	The identity matrix of size $N \times N$
κ	Carrier frequency of the systems used in the simulations
τ_c	The number of samples in a coherence block
τ_d	The number of samples allocated to the downlink data transmission
τ_p	The number of samples allocated to the uplink pilot transmission
τ_u	The number of samples allocated to the uplink data transmission
T_c	The coherence time of the systems

Acknowledgements

First, I would like to express my gratitude to my supervisors, Prof. Claude Oestges and Prof. Luc Vandendorpe, for their invaluable advices as well as the assistance and time they have generously provided me with over the past few months.

I would like to say a special thank you to Charles Wiame for his regular support from the very beginning. His passion for related subjects and his eargerness to share his knowledge were a great source of motivation.

I am also grateful to Prof. Jérôme Louveaux for taking the time he dedicates as a reader of this master thesis.

Computational resources have been provided by the supercomputing facilities of the Université catholique de Louvain (CISM/UCL) and the Consortium des Équipements de Calcul Intensif en Fédération Wallonie Bruxelles (CÉCI) funded by the Fond de la Recherche Scientifique de Belgique (F.R.S.-FNRS) under convention 2.5020.11 and by the Walloon Region. Thanks to them for providing students with such useful and valuable equipment.

ChatGPT has been used through this document as a tool for increasing the richness of vocabulary as well as the visual quality of the page layout and the various graphs.

Thank you to all my friends and especially to Sophie, Ottilie and Antoine, without whom this academic journey would not have had the same flavour.

Last but not least, I would like to express my deepest thanks to my parents who, for as long as I can remember, have given me everything they had to enable me to fulfil my potential and achieve my goals.

1

Introduction

In addition to its primary role in meeting the communication requirements of both humans and intelligent machines, networks surpassing the capabilities of 5G are poised to become an integral component of all parts of our society. These advanced networks will serve as a catalyst for materializing new technological aspirations like the Internet of Everything [1]. In pursuit of these objectives, the forthcoming era of networks beyond 5G is set to harness cutting-edge technologies, ushering in a new era of wireless communications characterized by unparalleled effectiveness and efficiency. This evolution promises an unprecedented surge in data rates, facilitating massive connectivity, ensuring high-reliability, and achieving low-latency communication capabilities [2].

When any new technology is introduced, the priority remains the safety of citizens. When it comes to advances in telecommunications networks, the question of the dangers of excessive exposure to EMF systematically comes up, and rightly so. Which is why it is essential to study the limits that can be reached in terms of performance in conjunction with the exposure provided by such systems.

Present mobile networks adhere to a cellular architecture, where each user equipment (UE) establishes a connection with a specific Base Station (BS), typically the one offering the strongest signal. The designated areas in which a particular BS serves UEs are termed cells. This kind of network provide good performance but relatively inconsistent. Indeed, a UE close to the boundary between two cells will experience strong interference from neighbouring BSs. However, cell-free networks began to emerge around 2015 as a new paradigm to meet this need for ever more homogeneous and high-performance cover.

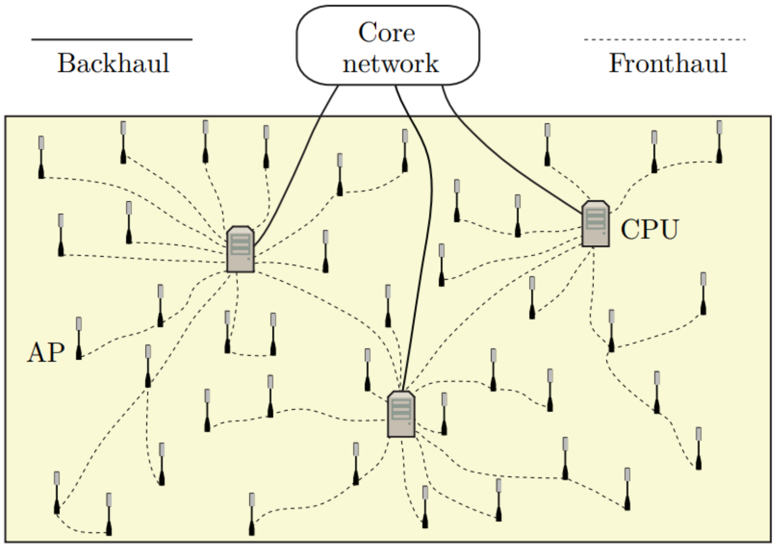

Figure 1.1: Example of cell-free network where the APs are randomly deployed and connected to CPUs using fronthaul (wired of wireless) links [3].

A cell-free network consists of densely and spatially distributed access points (i.e., more APs than UEs). Each AP has one or a few antennas. All network UEs are served by all APs. This approach eliminates traditional cell-edges, hence the designation of a "cell-free" framework. This concept is frequently associated with Massive Multiple-Input Multiple-Output (mMIMO) network principles. An example of such a network is illustrated in Figure 1.1. The user-centric cell-free architecture is a practical way to implement a cell-free network where UEs are no longer served by only a subset of the network's APs.

The increasing interest in this technology stems from its perceived role as a key driver for future mobile networks. Figure 1.2 illustrates the growing number of publications related to the subject since 2015.

The fundamental differences between cellular and cell-free networks can provide several key advantages. First, the spatially extensive deployment of distributed APs leads to a substantial increase in spatial degrees of freedom, enabling an enhanced capacity to serve a large number of UEs concurrently. Second, the dense deployment inherently facilitates significant interference mitigation, a critical factor for meeting the strict quality-of-service requirements in modern wireless networks. Third, the collaborative nature of distributed APs opens up new opportunities for cooperative transmission and reception, thereby enabling improved coverage and reliability. Table 1.1 summarizes key differences between cellular mMIMO cell-free mMIMO networks.

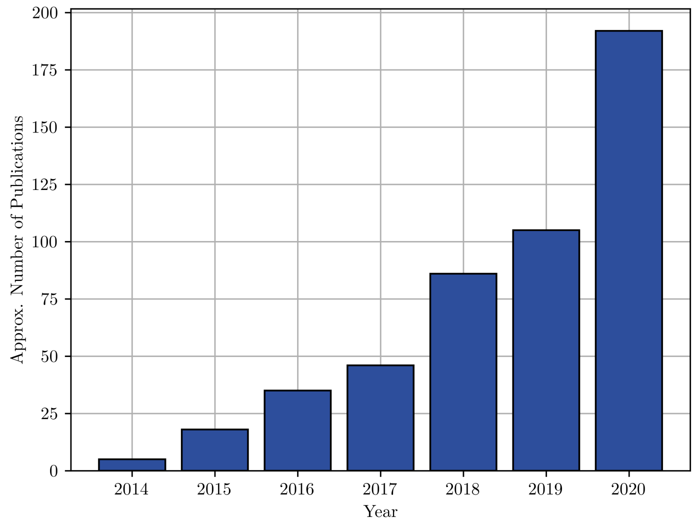

Figure 1.2: The increasing number of publications focusing on the cell-free network architecture reflects a significant and growing interest in this topic. It is noteworthy that the term *Cell-free* began to emerge in the literature around the year 2015, signaling a relatively recent but rapidly expanding research trend in the field [4].

Technology	**Cellular mMIMO**	**CF mMIMO**
Coverage	Small	Large
Clustering	Network-centric	User-centric
	Disjoint	Partially overlapping
	Fixed	Dynamic
A UE served by	One BS	All surrounding APs
CSI for decoding	Instantaneous	Instantaneous or statistical
Fronthaul load	-	Small
Synchronization	Uncritical	Critical
User-experience rate	Low	Large

Table 1.1: Comparison of the key differences between the two following network schemes: Cellular mMIMO and Cell-free mMIMO [5].

In this document, we attempt to compare the performance of cellular and cell-free networks in terms of spectral efficiency and EMF exposure in downlink operations. The aim is to see whether it is theoretically possible to achieve spectral efficiency levels similar to those offered by cellular in cell-free networks for a given exposure. These comparisons are made using numerical simulations. The document is organized as follows. Chapter 2 provides a review of the literature on cellular and cell-free networks, as well as an overview of issues relating to the EMF exposure including the possible metrics that can describe it as well as the limits fixed by the authorities. Chapter 3 describes the cellular mMIMO system model including network topology, channel modeling, channel estimation and the downlink performance metrics used in the simulations. The Cell-free mMIMO system model is presented in Chapter 4. It defines the User-Centric Dynamic Cooperation Clustering (DCC), the network topology, the channel modeling, the channel estimation and the downlink operation. Both types of networks are compared in Chapter 5 using the results obtained by the different numerical simulations. A pilot assignement technique is proposed in Chapter 6 and is compared with two other schemes. Concluding remarks and lessons learned in this work are provided in Chapter 7.

2

State of the Art

2.1 Cellular mMIMO Networks

To ensure the provision of wireless services with optimal signal reception over large coverage areas, the need for a cellular network topology was proposed in [6]. This concept involves subdividing the coverage area into cells, each operating autonomously with a fixed BS (the part of the network that allows the wireless communication with remote UEs). The evolution and analysis of the cellular network idea has been further developed over the decades [7, 8], before being deployed in practical applications. The concept of cellular networks represents a major advance and has played a central role in the provision of wireless services over the last forty years [9]. Originally intended for wireless voice communications, cellular networks are now predominantly driven by wireless data transmissions [10].

Cellular MIMO networks can deliver high data rates with a relatively good energy efficiency. It is also able to enhance the coverage and the link reliability as discussed in [11]. [12] proposes simple techniques for detection and precoding that can be used at a BS level for uplink and downlink operations. A first improvement of such networks was the cell densification (i.e. increasing the number of BSs, and therefore cells, per square kilometer) [13]. Another major improvement of cellular MIMO networks, which emerged later, is the introduction of massive MIMO which means making use of a large number of antennas per BS. Some say that this innovation was introduced by Thomas Marzetta in 2010. Massive MIMO is widely discussed in [14, 15]. Use a large number of antennas per BS can lead to huge performance improvement due to the spatial multiplexing and the inter-users interference cancellation that it allows [16, 17]. Today, one of the main limitations of cellular networks is their lack of uniformity in terms of coverage [3].

2.2 Cell-Free mMIMO Networks

Cell densification of cellular networks has shown some limitations. Indeed when there are 10 or more BSs per km^2, the inter-cell interference starts to grow and can even become dominant [18]. In contrast from co-located mMIMO networks (or cellular networks), mMIMO operation can also be implemented in a distributed manner by deploying a large number of geographically dispersed AP with single or multiple antennas, connected to a CPU through high-speed fiber or wireless fronthaul links [19]. This is what we call cell-free networks these days. This designation comes from [20]. The goal of cell-free networks is therefore to provide a dense network (with more APs than UEs) where the concept of inter-cell interference is no longer and to offer the most uniform data rates possible in the network area [5]. The concept of *user-centric cell-free networks*, introduced in Chapter 1 and developed in Section 4.1.1 is defined and compared with the native definition of cell-free networks in [21]. Tutorials/surveys on the operating principles of cell-free mMIMO networks are provided in [3, 4, 22]. In user-centric cell-free mMIMO networks, UEs are served by a fraction of the network's APs. The way these subsets of APs are defined is called *cooperation clustering*. In the network setup considered in this document, the cooperation clustring works in conjuction with the pilot assignement. A pilot is assigned to each UE in order to enable CPUs to estimate the channel. This is developed in Section 4.1.4. [23] provides a scalable cooperation clustering techniques as well as two innovative scalable pilot assignement schemes. In [24], several practical deployement issues, like radio stripes systems, synchronization, fronthaul/backhaul capacity, of ubiquitous cell-free mMIMO communication systems are discussed. Furthermore, the study of cell-free mMIMO performance under several practical constraints is proposed in [25].

2.3 EMF Exposure

When talking about EMF exposure the distinction between non-ionizing radiations and ionizing radiations must be done [26]. These two kinds of radiations are represented on the electromagnetic spectrum in Figure 2.1.

The former one is a *low-frequency* electromagnetic radiation (or at least at a lower frequency than the second) whose photons do not carry enough energy to modify the structure of the DNA. These are the electromagnetic radiations

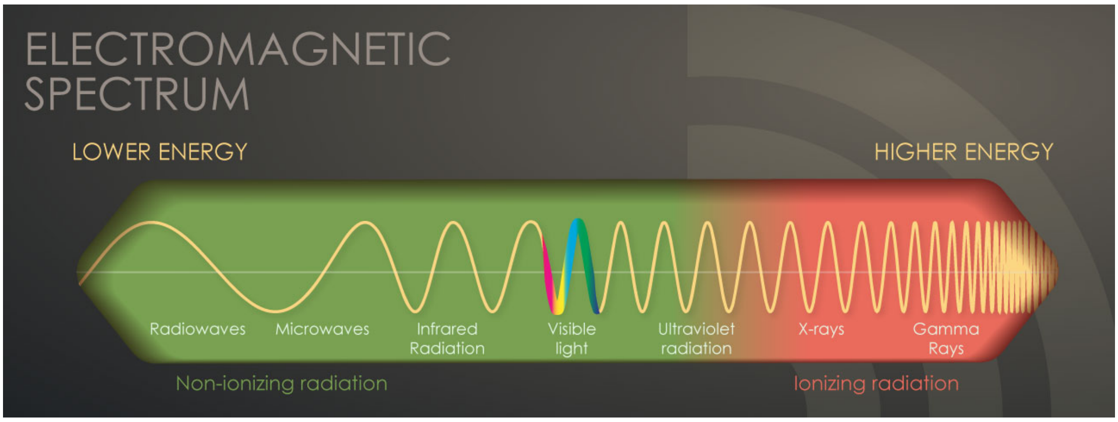

Figure 2.1: Electromagnetic spectrum illustrating non-ionizing radiation (on the left) and ionizing radiation (on the right) [27].

used in telecommunication networks and that are therefore considered in this document. However, those waves can have enough energy to heat the cells by vibrating the molecules. This could potentially cause health issue. An example of EMF source causing thermal effects is the microwave oven, even though its primary purpose is not for RF communications. Within this context, the mechanism leading to an increase in temperature of the exposed tissues is deeply understood and widely examined in the literature [28]. Obviously, such a high level of heating is not expected when talking about communication networks. Indeed, in order to avoid any heating effect, regulatory authorities like the European Commission or International commission on non-ionizing radiation protection (ICNIRP), have set exposure limits that operators cannot exceed as explained in Section 2.3.2.

The ionizing radiations at higher frequency, can carry enough energy to modify the structure of the DNA [29]. They start on the spectrum at the level of the UV-B ($\lambda = 290$ to 320 nm).

In communication networks, the UEs are mainly exposed to EMF coming from two sources : from the BSs (or AP in cell-free) in downlink and from the UEs themselves in uplink. This is illustrated in Figure 2.2. In general, the main source of exposure coming from UEs are themselves by using mobile devices. The resulting EMF are localized either on the head or chest. When the EMF comes from BSs (or APs) it is radiated much further and over the entire body compared to when it comes from UEs.

In order to be compared with regulatory limits, EMF exposure measured values have to be extrapolated since they can vary considerably over time and according to the position of UEs. The general idea for estimating the EMF exposure in

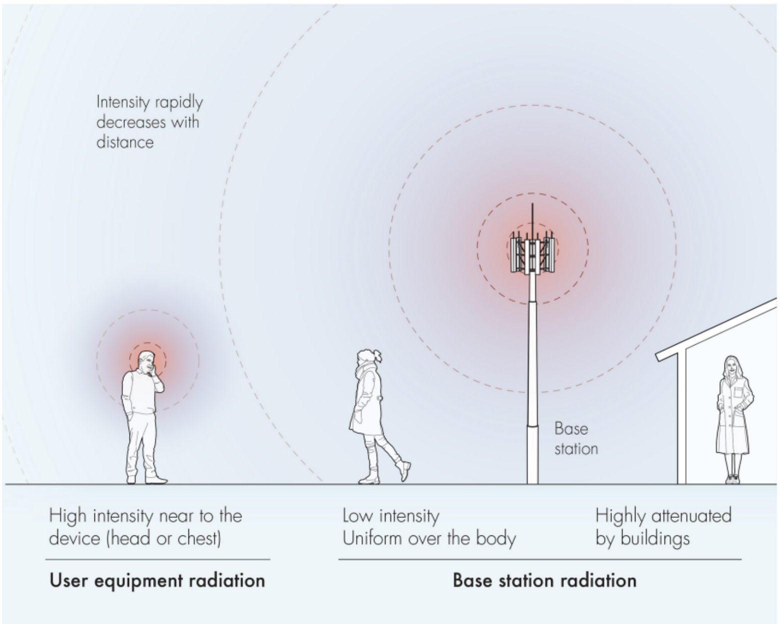

Figure 2.2: Illustration of the two main sources of EMF exposure in uplink on the left and downlink on the right.EMF exposure rapidly decreases with the distance and as shown by the white color in the building, it can be highly attenuated by obstacles [30].

communication networks relies on measuring the periodic signaling, which is consistently transmitted and unaffected by a BS's traffic load [31]. An overview of methods for assessing EMF exposure is provided by [32].

2.3.1 Exposure Metrics

The main exposure metrics that can be found in the literature nowadays are, according to [30],

1. EMF strength
2. Incident power density
3. Specific absorption rate (SAR)

In the following subsections, these metrics are briefly defined.

Electromagnetic Field Strength

Every radio frequency (RF) emitter releases an electromagnetic field (EMF) that spans the nearby surroundings. This field consists of both an electric component, denoted as **E** [V/m], and a magnetic component, denoted as **H** [T]. It is measured in volt per meter [V/m]. The EMF strength limits for several carrier frequency fixed in the Walloon region are given in Table 2.1.

Specific Absorption Rate

The SAR is a measurement that quantifies the rate at which the human body absorbs electromagnetic energy upon exposure to RF signals. [30]. SAR is a crucial parameter in assessing potential health risks associated with the use of wireless communication devices. It is a metric that usually dominates when dealing with rather low radio frequencies. When dealing with frequencies exceeding one gigahertz, the EMF absorption starts to become superficial and this is why IPD restrictions are commonly applied in downlink transmissions instead of SAR [33].

Incident Power Density

The incident power density (IPD) defined as the exposure in (3.21) for cellular networks and in (4.29) for cell-free networks is the power of an electromagnetic wave incident on a unit area. It is expressed in watt per square meter (W/m^2). This is the metric used in this document in order to compare the exposure between the two types of networks. IPD is well suited when working with high frequencies. It has therefore been selected as the reference metric, given that cell-free networks will be required to operate at high frequencies [34, Section 3.2].

2.3.2 Exposure Limits

As mentioned earlier, radio waves are subject to exposure limits : the maximum amount of electromagnetic radiation to which a citizen may be exposed. These limits are determined by regulatory authorities (e.g. the Federal Communications Commission (FCC) in the USA or the European Commission in Europe) or international commissions (e.g. ICNIRP)

A lot of studies have been carried out in order to evaluate the risks of the radiations on humans, depending on the type of radiation, its intensity and the duration of exposure. Those studies have established limits that must not be exceeded in order to prevent health risks. Additional reduction factors can also be applied in order to take into account children, pregnant women, the elderly and the sick. These restrictions are regularly re-evaluated and modified if necessary. **Nowadays, no study has demonstrated that respecting these limits poses a health risk to humans.**

Extreme vigilance is still required when dealing with new technologies or new bandwidth hence the importance of studying the exposure in cell-free networks.

Carrier frequency [MHz]	EMF [V/m]	IPD [W/m^2]	Application example
700	16.2	0.696	5G
800	17.4	0.803	4G/5G
900	18.4	0.898	2G/3G/5G
1800	26	1.793	2G/4G/5G
2100	27.4	1.991	3G/4G/5G
2400	27.4	1.991	Wi-Fi
2600	27.4	1.991	4G/5G
3500	27.4	1.991	4G/5G
5200	27.4	1.991	Wi-Fi

Table 2.1: Cumulative limits of the EMF (that takes into account all the influences of nearby antennas) fixed by the Walloon region in Belgium [35]. These limits are different depending on the regions. They are based on the recommendations of the Council of the European Union and the ICNIRP

Table 2.1 sums up the exposure limits for a range of frequencies that are in place in the Walloon Region in Belgium. They are set at regional level and may therefore differ in the Flemish Region or the Brussels-Capital Region.

Even if no health diseases linked to EMF exposure have been demonstrated the subject remains highly controversial and several **alleged** health effects can be enumerated:

- Cancer
- Skin Effects
- Ocular Effects
- Glucose metabolism
- Male Fertility
- Electromagnetic Hypersensitivity

This is a non exhaustive list. These effects are explained in greater depth in [30, Section II.B].

Metric	Notation
CCDF of the coverage	$\bar{F}_{\mathrm{SE}}(T)$
CCDF of the EMF exposure	$\bar{F}_{\xi}(T')$
Conditional CCDF of the coverage-EMF exposure	$\bar{F}_{\mathrm{SE}\mid\xi}(T\mid T')$
Joint CCDF of the coverage-EMF exposure	$\bar{F}_{\mathrm{SE},\xi}(T,T')$
Meta distribution of the coverage	$\mathcal{F}_{\mathrm{SINR}}(s,T)$
Meta distribution of the EMF exposure	$\mathcal{F}_{\xi}(s,T')$

Table 2.2: Overview of the metrics used to compare the performances of cellular and cell-free networks. These are defined in Section 5.1.1.

2.4 Contributions

The main contributions of this document are summarized as follows

- In Chapter 3 and 4, after a description based on the works provided in respectively [9] and [3] of the system models used to compare cellular and cell-free networks, expressions of average SE, instantaneous SINR and EMF exposure (expressed by the IPD) are proposed for downlink operations using perfect CSI.
- A numerical analysis and comparison of the average SE and EMF exposure achievable in cellular and cell-free networks is provided in Chapter 5. This is performed using several metrics summarized in Table 2.2[1].
- An efficient pilot assignement technique, in term of computational complexity, based on the K-Means clustering of deployed APs is proposed in Chapter 6. The performances are compared with the ones of two other pilot assignement schemes.
- Finally, some avenues of future research potentially capable of improving the quality and depth of the analyses proposed in this document are discussed in the conclusion.

[1]Some of the notations summarized in this table are inspired by [36, Table 2.1]

3

System Model : Cellular mMIMO Networks

In this chapter, the system model of a simple cellular network (composed of 4 cells in a wrap-around topology) is described. Section 3.1 covers the simulation requirements that are used to obtain the numerical results summarized in Chapter 5 such as the network topology, the channel modeling and channel estimation. Section 3.2 defines the expressions of the spectral efficiency, SINR and exposure that are used to compare the performance of cellular networks with that of cell-free networks.

3.1 Simulation Requirements

This section, as well as the beginning of Section 3.2, are based on the work proposed in the book *Massive MIMO Networks: Spectral, Energy, and Hardware Efficiency* [9].

3.1.1 Network Topology

During the simulations, the cellular network is deployed as shown in Figure 3.1. Each cell is a 0.5 km × 0.5 km square cell in a wrap-around arrangement. The number of cells is equal to $L = 4$.

The number of UEs K in the network is fixed to $K = 40$ and the number of UEs per cell is the same for each cell and equal to $K_j = 10 \; \forall j$. The UEs are deployed

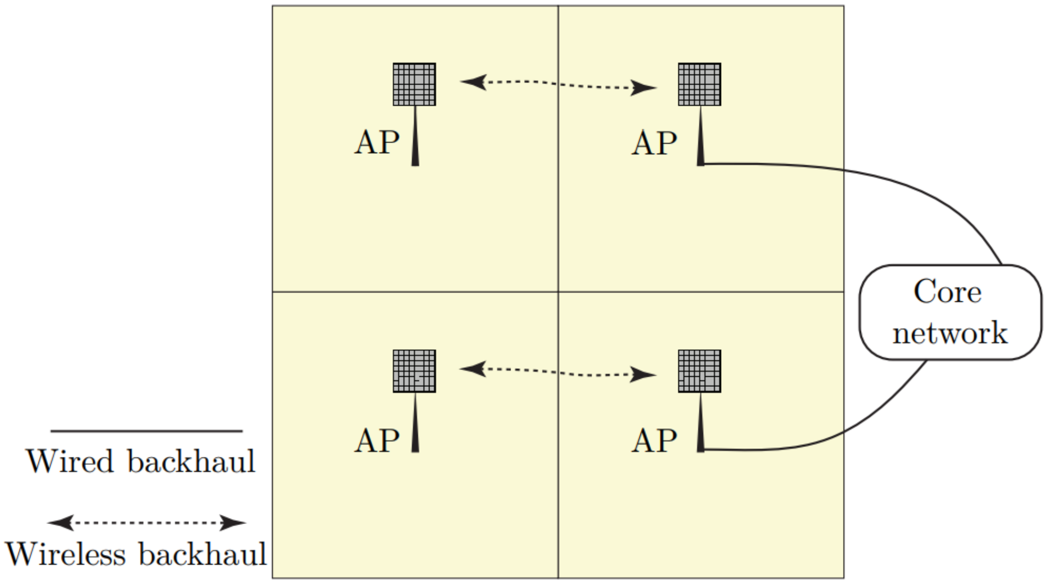

Figure 3.1: Illustration of the cellular network topology used in the simulation. It contains 4 BS each standing in the center of their 0.5 km $\times$ 0.5 km cell [3].

randomly in each cell (with K_j UEs per cell) and their positions are uniformly distributed :

$$[x_{jk}, y_{jk}] \sim \mathcal{U}_{[0,0.5]} \tag{3.1}$$

The number N_j of antennas per BS is the same for each BS and equal to $N_j = 100\ \forall j$.

3.1.2 Channel Modeling

This section describes the channel model used in the simulations of cellular mMIMO networks.

Block fading and Coherence Blocks

Figure 3.2 illustrates a coherence block. A coherence block is a time-frequency interval characterized by a temporal duration equivalent to the coherence time T_c and a frequency bandwidth equivalent to the coherence bandwidth B_c (the total number of samples inside a block $\tau_c = B_c T_c$). The dimensions of a coherence block can vary according several parameters such as the carrier frequency or the channel delay spread.

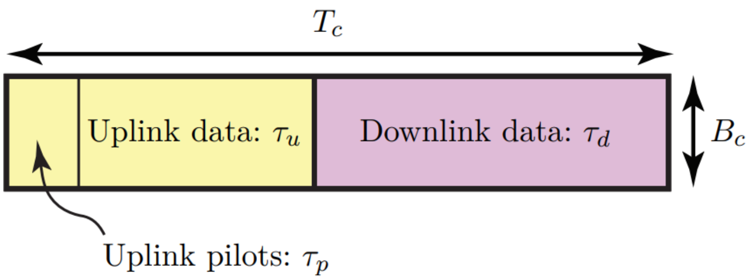

Figure 3.2: Representation of a coherence block when using a TDD protocol. It is divided into three part : uplink pilot transmission, uplink data transmission and downlink data transmission [3].

In this document, the coherence block size has been calculated using the following approximations $T_c = \lambda/4v$ and $B_c = 1/(2T_d)$ [37] where v is the maximum speed at which a device is expected to move, and T_d is the channel delay spread. The worst-case scenario is considered here to avoid ending up with a "too large" coherence block. Considering a carrier frequency $\kappa = 2$ GHz, a maximum speed of $v = 135$ km/h, and a channel delay spread of 2.5μs (which is relatively high for an urban area [38]), the resulting size is $\tau_c = 200$. Inside this block, it is assumed that the channel is constant and that it is the same in both uplink and downlink (channel reciprocity). This hypothesis is considered as true in both the cellular and cell-free part of the document.

The block is divided into three parts. The first one is allocated to the transmission of the uplink pilot signals. These signals will be used to compute the estimation of the channels by the BSs as explained in Section 3.1.3.

The two remaining parts are the fraction of the coherence block used for both uplink and downlink data transmission. In the context of this document, it is considered that the BSs estimate the channel vectors (used to compute precoding vectors as explained below) whereas the UEs have knowledge of the perfect CSI which is an idealized assumption. In reality, obtaining perfect and instantaneous knowledge of the channel conditions is challenging due to various factors such as signal fading and interference.

Correlated Rayleigh Fading

In the cellular part of this document, each UE is indexed by the number l of the cell it is part of ($l \in L$ with L the number of cells/BS in the network) and it's own index k in this same cell ($k \in K_j$ with K_j the number of UEs in the cell j). Therefore, $\mathbf{h}_{lk}^{j} \in \mathbb{C}^{N_j}$ (with N_j being the number of antennas in the BS of cell j)

denotes the channel response between the UE k in cell l and the BS j. In other words, the subscript is the cell and index of the UE while the superscript provides the index of BS.

It is considered that some directions are more probable to carry strong signals between the BSs and the UEs in the physical propagation environment. Therefore, the channels are defined as spatially correlated in the simulations. This means that their distribution is characterized by the correlation matrix $\mathbf{R}_{lk}^{j}$ and not only by fading coefficients, as described in (3.2). This channel model is said to be *Rayleigh* since the magnitude $|h_{lk_n}^{j}|\ \forall n \in N_j$ is distributed according to a Rayleigh distribution. The channel vectors are distributed as

$$\mathbf{h}_{lk}^{j} \sim \mathcal{N}_{\mathbb{C}}\left(\mathbf{0}_{N_j}, \mathbf{R}_{lk}^{j}\right) \tag{3.2}$$

where $\mathbf{R}_{lk}^{j} \in \mathbb{C}^{N_j \times N_j}$ is the spatial correlation matrix. The (m,ℓ)th element of $\mathbf{R}$ is given by

$$[\mathbf{R}]_{m\ell} = \beta \int\int e^{j\pi(m-\ell)\sin(\varphi)\cos(\theta)} f(\varphi,\theta) d\varphi d\theta \tag{3.3}$$

where φ and θ are respectively the azimuth and elevation angles. $f(\varphi,\theta)$ is the joint PDF of φ and θ (here a joint normal distribution is considered). Scatters are considered as being located only around the UEs since the BSs (or APs in cell-free) are supposed to be surrounded by obstacles because they are placed high up. It is assumed that every BS have access to these matrices at all time. The small-scale fading variations are modeled by the Gaussian distribution. It is assumed that in each coherence block the simulation computes a new independent realization from this distribution to model the channel response. Conversely, the spatial correlation matrix describes the macroscopic propagation effects at both the transmitting and receiving ends.

Large-Scale Fading Model

The following large-scale fading coefficient β_{lk}^{j} model will be used in the simulations in order to compute the correlation matrices $\mathbf{R}_{lk}^{j}$:

$$\beta_{lk}^{j}[\text{dB}] = -35.3 - \underbrace{37.6}_{10\alpha} \log_{10}\left(\frac{d_{lk}^{j}}{1\text{m}}\right) + F_{lk}^{j} \tag{3.4}$$

where d_{lk}^{j} [m] is the distance between the BS j and the UE k in cell l. d_{lk}^{j} is always greater than 35 m. The signal power is attenuated with the distance and this rate

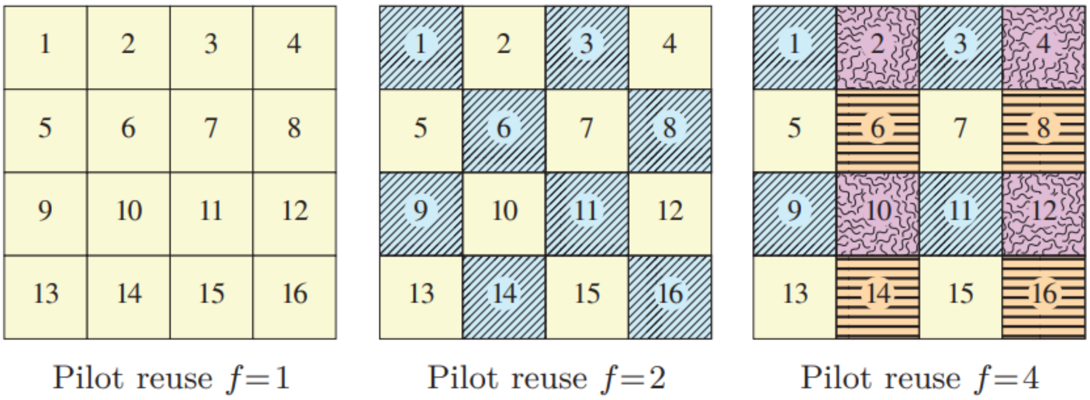

Figure 3.3: Illustration of a 4×4 cells cellular network with different pilot reuse factor [9].

of decline is determined by the pathloss exponent α [9, Section 2.2]. The shadow fading is modeled by $F_{lk}^{j} \sim \mathcal{N}(0, \sigma_{\text{sf}}^2)$.

3.1.3 Channel Estimation

The channel estimation is performed in the uplink using pilot signals as described in the following subsections. The channel estimates are used by the BSs to compute the precoding vectors $\mathbf{w}_{jk}$. In the downlink, UEs have perfect knowledge of the CSI.

Uplink pilot transmission

To optimize the utilization of the large number of antennas in the arrays, every BS must estimate the channel responses from the active UEs within the current coherence block. To this end, a pilot signal sent by UEs are used by the BSs. τ_p samples are allocated to the uplink pilot transmission. A *pilot sequence*, spanning the assigned τ_p samples, is designated for each UE. In the simulations $\tau_p = K_j = 10$ and the *pilot reuse factor* is equal to $f = 1$. It is considered that $\tau_p = fK_j$. The fact that in the simulations $\tau_p = K_j = 10$ and $f = 1$ means that there is no intra-cell pilot contamination (since the pilot signal of each UE is orthogonal to the one of the other UEs belonging to the same cell) but UEs will experience inter-cell interference. Indeed, there are as many orthogonal pilot sequences into a cell as there are UEs (for example the rows of $\mathbf{I}_{\tau_p}$). An illustration of a network with different pilot reuse factor is given in Figure 3.3.

In the case where the pilot reuse factor is equal to $f = 1$, every cell uses the same set of pilot sequences, this is why UEs will experience inter-cell pilot contamination.

The received pilot signal $\mathbf{Y}_l^{\text{pilot}} \in \mathbb{C}^{N_j \times \tau_p}$ at BS j during the entire pilot transmission (hence its dimensions $\mathbb{C}^{N_j \times \tau_p}$) is given by

$$\mathbf{Y}_j^{\text{pilot}} = \underbrace{\sum_{k=1}^{K_j} \sqrt{p_{jk}} \mathbf{h}_{jk}^j \boldsymbol{\phi}_{jk}^{\mathrm{T}}}_{\text{Desired pilots}} + \underbrace{\sum_{\substack{l=1 \\ l \neq j}}^{L} \sum_{i=1}^{K_l} \sqrt{p_{li}} \mathbf{h}_{li}^j \boldsymbol{\phi}_{li}^{\mathrm{T}}}_{\text{Inter-cell pilots}} + \underbrace{\mathbf{N}_j}_{\text{Noise}} \tag{3.5}$$

where $p_{jk} \geq 0$ is the uplink power of UE k in cell j and $\mathbf{N}_j$ is an independent additive noise.

By making use of the mutually orthogonal nature of the pilot signals, the BS j will be able to estimate the channel between itself and UE i in cell l i.e. $\mathbf{h}_{li}^j$. Multiplying $\mathbf{Y}_j^{\text{pilot}}$ with $\boldsymbol{\phi}_{jk}$ of the corresponding UE gives, in the case where the UE is belonging to the same cell as the BS[1] j, the processed received pilot signal $\mathbf{y}_{jjk}^{\text{pilot}} \in \mathbb{C}^{N_j}$

$$\begin{aligned}
\mathbf{y}_{jjk}^{\text{pilot}} &= \mathbf{Y}_j^p \boldsymbol{\phi}_{jk}^* \\
&= \underbrace{\sqrt{p_{jk}} \mathbf{h}_{jk}^j \boldsymbol{\phi}_{jk}^{\mathrm{T}} \boldsymbol{\phi}_{jk}^*}_{\text{Desired pilot}} + \underbrace{\sum_{\substack{i=1 \\ i \neq k}}^{K_j} \sqrt{p_{ji}} \mathbf{h}_{ji}^j \boldsymbol{\phi}_{ji}^{\mathrm{T}} \boldsymbol{\phi}_{jk}^*}_{\text{Intra-cell pilots}} + \underbrace{\sum_{\substack{l=1 \\ l \neq j}}^{L} \sum_{i=1}^{K_l} \sqrt{p_{li}} \mathbf{h}_{li}^j \boldsymbol{\phi}_{li}^{\mathrm{T}} \boldsymbol{\phi}_{jk}^*}_{\text{Inter-cell pilots}} \\
&\quad + \underbrace{\mathbf{N}_j^p \boldsymbol{\phi}_{jk}^*}_{\text{Noise}}
\end{aligned} \tag{3.6}$$

The inner product $\boldsymbol{\phi}_{li}^{\mathrm{T}} \boldsymbol{\phi}_{jk}^*$ appears in the second and third term in (3.6). When the pilot sequences in the product are orthogonal, it is equal to $\boldsymbol{\phi}_{li}^{\mathrm{T}} \boldsymbol{\phi}_{jk}^* = 0$. As mentioned earlier, every UE in a given cell have orthogonal pilot sequences. This is an assumption made in this document since it has been decided that $\tau_p = K_j$ but it can be false in other conditions. This is why the second term will always be zero and there will be no intra-cell pilot contamination. This is not true for the third term. Ideally, all the pilot sequences should be orthogonal. However this means that τ_p should be increased and that would lead to a decrease of the spectral efficiency since less symbols per coherence block would be assigned to useful transmission.

[1]The expression of $\mathbf{y}_{jli}^{\text{pilot}}$ for $l \neq j$ is described in [9, Section 3.1].

MMSE Channel Estimation

The channel are estimated by the BS by using MMSE estimation. The MMSE estimator of $\mathbf{h}_{li}^{j}$ minimizes the MSE $\mathbb{E}\{||\mathbf{h}_{li}^{j} - \widehat{\mathbf{h}}_{li}^{j}||^2\}$. Theorem 3.1 details the MMSE estimation.

Theorem 3.1. When the UEs in the network employ pilot sequences that are mutually orthogonal, the MMSE estimation of the channel $\mathbf{h}_{li}^{j}$ is performed using $\mathbf{Y}_j^{\text{pilot}}$, defined in (3.5), as follows

$$\widehat{\mathbf{h}}_{li}^{j} = \sqrt{p_{li}}\mathbf{R}_{li}^{j}\left(\boldsymbol{\Psi}_{li}^{j}\right)^{-1}\mathbf{y}_{jli}^{\text{pilot}} \tag{3.7}$$

where

$$\boldsymbol{\Psi}_{li}^{j} = \sum_{(l',i')\in\mathcal{P}_{li}} p_{l'i'}\tau_p\mathbf{R}_{l'i'}^{j} + \sigma_{\text{ul}}^2\mathbf{I}_{M_j} \tag{3.8}$$

is the correlation matrix of the processed pilot signal in (3.6). And the set (used in (3.8)) containing the indices of all UEs sharing the same pilot as UE k in cell j, including itself, is given by

$$\mathcal{P}_{jk} = \{(l,i) : t_{li} = t_{jk}, \quad l = 1, ..., L; \quad i = 1, ..., K_l\} \tag{3.9}$$

where t_{li} is the pilot index of UE i in cell l.

The error correlation matrix $\mathbf{C}_{li}^{j} = \mathbb{E}\left\{\widetilde{\mathbf{h}}_{li}^{j}(\widetilde{\mathbf{h}}_{li}^{j})^{\text{H}}\right\}$ with $\widetilde{\mathbf{h}}_{li}^{j} = \mathbf{h}_{li}^{j} - \widehat{\mathbf{h}}_{li}^{j}$ (the error of estimation) is given by

$$\mathbf{C}_{li}^{j} = \mathbf{R}_{li}^{j} - p_{li}\tau_p\mathbf{R}_{li}^{j}\boldsymbol{\Psi}_{li}^{j}\mathbf{R}_{li}^{j} \tag{3.10}$$

The theorem can be found in [9, Section 3.2] and the proof in [9, App. C.2.1].

This theorem provides the way the BSs estimate the channels between them and the UEs of the network using the uplink pilot signal. Those estimates are used in order to compute the precoding vectors. As mentioned earlier, in the downlink, it is however considered that the UEs have perfect knowledge of the CSI.

3.2 Downlink Operation

In the downlink operation, the signal transmitted by the BS in cell l is denoted $\mathbf{x}_l \in \mathbb{C}^{N_l}$. The received signal $y_{jk}^{\text{dl}} \in \mathbb{C}$ at UE k in cell j can then be written as

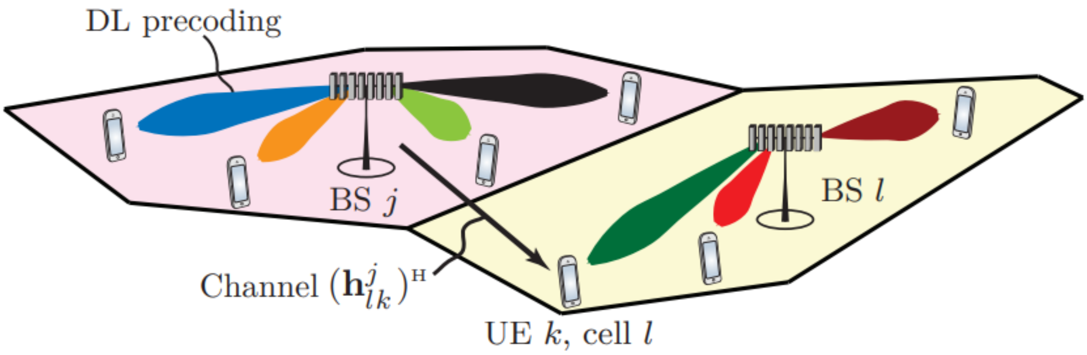

Figure 3.4: Illustration of the downlink mMIMO operation in cell j and cell l. $\left(\mathbf{h}^j_{lk}\right)^{\mathrm{H}} \in \mathbb{C}^{N_j}$ denotes the channel vector between BS j and UE k in the cell l [9].

$$y^{\mathrm{dl}}_{jk} = \sum_{l=1}^{L} (\mathbf{h}^l_{jk})^{\mathrm{H}} \mathbf{x}_l + n_{jk} \tag{3.11}$$

where $n_{jk} \sim \mathcal{N}_{\mathbb{C}}(0, \sigma^2_{\mathrm{dl}})$ is the noise with variance σ^2_{dl}. The downlink channel is represented by $(\mathbf{h}^l_{jk})^{\mathrm{H}}$. While in practice, a transpose is used and not a complex conjugate in $(\mathbf{h}^l_{jk})^{\mathrm{H}}$, it is used to simplify the notation. Consequently, this will be the notation used in this document, in both the cellular part and in the cell-free part.

The signal transmitted by BS l can be written as

$$\mathbf{x}_l = \sum_{i=1}^{K_l} \mathbf{w}_{li} \varsigma_{li} \tag{3.12}$$

where $\varsigma_{lk} \sim \mathcal{N}_{\mathbb{C}}(0, \rho_{lk})$ is the downlink data signal that is transmitted through $\mathbf{x}_l$ for UE k in the cell l and ρ_{lk} is power of this signal. In order to perform beamforming and assign a particular spatial directivity to the signal $\mathbf{x}_l$, a precoding vector $\mathbf{w}_{lk} \in \mathbb{C}^{M_l}$ is multiplied with the data. It should be noted that $\mathbb{E}\{||\mathbf{w}_{lk}||^2\} = 1$ and therefore $\mathbb{E}\{||\mathbf{w}_{lk}\varsigma_{lk}||^2\} = \rho_{lk}$ which is the transmit power that BS l allocates to this UE. An example of such a downlink transmission is illustrated in Figure 3.4.

By substituting the transmitted signal in (3.12) into (3.13) and by extracting the index $i = k$ from the sum, the received downlink signal at UE k becomes

$$
\begin{aligned}
y_{jk}^{\mathrm{dl}} &= \sum_{l=1}^{L}\sum_{i=1}^{K_l}(\mathbf{h}_{jk}^{l})^{\mathrm{H}}\mathbf{w}_{li}\varsigma_{li} + n_{jk} \\
&= \underbrace{(\mathbf{h}_{jk}^{j})^{\mathrm{H}}\mathbf{w}_{jk}\varsigma_{jk}}_{\text{Desired signal}} + \underbrace{\sum_{\substack{i=1\\ i\neq k}}^{K_j}(\mathbf{h}_{jk}^{j})^{\mathrm{H}}\mathbf{w}_{ji}\varsigma_{ji}}_{\text{Intra-cell interference}} + \underbrace{\sum_{\substack{l=1\\ l\neq j}}^{L}\sum_{i=1}^{K_l}(\mathbf{h}_{jk}^{l})^{\mathrm{H}}\mathbf{w}_{li}\varsigma_{li}}_{\text{Inter-cell interference}} + \underbrace{n_{jk}}_{\text{Noise}}
\end{aligned} \tag{3.13}
$$

The downlink separation of the UEs is performed using *space-division multiple access* (SDMA).

3.2.1 Precoding Vectors

This section provides the expressions of the four precoding vectors (others exist) used in the cellular simulations in Chapter 5.

MR

The first option, which does not take interference into account, is the MR precoding.

$$
\mathbf{w}_{jk}^{\mathrm{MR}} = \frac{\mathbf{h}_{jk}^{j}}{||\mathbf{h}_{jk}^{j}||} \tag{3.14}
$$

This scheme will lead to the poorest performance in terms of SE as illustrated in Chapter 5.

M-MMSE

The multi-cell MMSE (M-MMSE) minimizes the mean square error between the data and the received signals intended for every UE.

$$
\mathbf{w}_{j}^{\text{M-MMSE}} = \left[\mathbf{w}_{j1}, ..., \mathbf{w}_{jK_j}\right]^{\mathrm{T}} \tag{3.15}
$$

$$
= \left(\sum_{l=1}^{L}\widehat{\mathbf{h}}_{l}^{j}\mathbf{P}_{l}\left(\widehat{\mathbf{h}}_{l}^{j}\right)^{\mathrm{H}} + \sum_{l=1}^{L}\sum_{i=1}^{K_l}p_{li}\mathbf{C}_{li}^{j} + \sigma_{\mathrm{ul}}^{2}\mathbf{I}_{N_j}\right)^{-1}\widehat{\mathbf{h}}_{j}^{j}\mathbf{P}_{j} \tag{3.16}
$$

with $\mathbf{P}_l = \mathrm{diag}(p_{l1}, ..., p_{lK_l}) \in \mathbb{R}^{K_l\times K_l}$ containing the uplink transmit powers, $\widehat{\mathbf{h}}_{l}^{j} = \left[\widehat{\mathbf{h}}_{l1}^{j}, ..., \widehat{\mathbf{h}}_{lK_l}^{j}\right]^{\mathrm{T}} \in \mathbb{C}^{N_j\times K_l}$ containing the channel estimates between UEs in cell l and BS j and $\mathbf{C}_{li}^{j}$ defined in (3.10).

S-MMSE

Single-cell MMSE (S-MMSE) precoding vector of BS j is obtained from (3.15) by considering that each BS only estimates the channels between itself and UEs it serves.

$$\mathbf{w}_j^{\text{S-MMSE}} = \left(\widehat{\mathbf{h}}_j^j \mathbf{P}_j \left(\widehat{\mathbf{h}}_j^j \right)^{\mathrm{H}} + \sum_{i=1}^{K_j} p_{ji} \mathbf{C}_{ji}^j + \sigma_{\text{ul}}^2 \mathbf{I}_{N_j} \right)^{-1} \widehat{\mathbf{h}}_j^j \mathbf{P}_j \tag{3.17}$$

P-RZF

By considering that the correlation matrix is negligible in (3.17) (this can be the case when the amount of interference coming from other cells is low), P-RZF precoding vector for BS j can be expressed as follows

$$\mathbf{w}_j^{\text{P-RZF}} = \left(\widehat{\mathbf{h}}_j^j \mathbf{P}_j \left(\widehat{\mathbf{h}}_j^j \right)^{\mathrm{H}} + \sigma_{\text{ul}}^2 \mathbf{I}_{N_j} \right)^{-1} \widehat{\mathbf{h}}_j^j \mathbf{P}_j \tag{3.18}$$

3.2.2 Spectral Efficiency

In order to transmit payload data to the UEs, BSs use precoding vectors $\mathbf{w}_{jk} \in \mathbb{C}^{N_j}$ that determines the spatial directivity. A precoding vector is assigned to all UEs a BS is serving. Theorem 3.2 gives an achievable SE for the UEs that have perfect knowledge of the CSI.

Theorem 3.2. The expression of SE achievable by UE k in cell j in downlink when considering that the UE have knowledge of the perfect CSI is

$$\text{SE}_{jk}^{\text{dl}} = \frac{\tau_d}{\tau_c} \mathbb{E} \left\{ \log_2 \left(1 + \text{SINR}_{jk}^{\text{dl}} \right) \right\} \quad \text{[bit/s/Hz]} \tag{3.19}$$

where the instantaneous effective SINR is given by

$$\text{SINR}_{jk}^{\text{dl}} = \frac{\rho_{jk} \left| (\mathbf{h}_{jk}^j)^{\mathrm{H}} \mathbf{w}_{jk} \right|^2}{\sum\limits_{\substack{i=1 \\ i \neq k}}^{K_j} \rho_{ji} \left| (\mathbf{h}_{jk}^j)^{\mathrm{H}} \mathbf{w}_{ji} \right|^2 + \sum\limits_{\substack{l=1 \\ l \neq j}}^{L} \sum\limits_{i=1}^{K_l} \rho_{li} \left| (\mathbf{h}_{jk}^l)^{\mathrm{H}} \mathbf{w}_{li} \right|^2 + \sigma_{\text{dl}}^2} \tag{3.20}$$

The expectation in (3.19) is with respect to the channel realizations.

3.2.3 EMF Exposure

Starting from (3.20), one can derive the EMF exposure per UE in downlink. The incident power density (IPD) at UE k in cell j is given by

$$\xi_{jk} = \frac{4\pi}{\lambda^2} \sum_{l=1}^{L} \sum_{i=1}^{K_l} \rho_{li} \left| (\mathbf{h}_{jk}^{l})^{\mathrm{H}} \mathbf{w}_{li} \right|^2 \quad [\mathrm{W/m^2}] \tag{3.21}$$

This takes into account the contribution of the desired and interfering signals. $\lambda = c/\kappa$ is the carrier wavelength, with $\kappa = 2$ GHz the carrier frequency and c the speed of light in vacuum.

4

System Model : Cell-Free mMIMO Networks

This chapter describes the system model of a user-centric cell-free mMIMO network in the centralized downlink operation. Centralized mean that the CPU is responsible of the data encoding as well as the computation of the transmit precoding vectors as illustrated in Figure 4.2 where the APs only act as RRH (the distributed case is not studied in this document). Section 4.1 covers the simulation requirements such as the topology of the cell-free network and the way the channels are modeled and estimated. Section 4.2 defines the received downlink signals as well as the spectral efficiency, SINR and EMF exposure.

4.1 Simulation Requirements

The system model described in this chapter is based on the one given in the book *Foundations of User-Centric Cell-Free Massive MIMO* [3].

Important note : Unlike cellular networks where each UE is indexed by the number of the cell in which it is located and its own number in this same cell (as described in chapter 3), in the cell-free networks, each UE has only one index (it's own number). Therefore where we used to denote the canal between the BS in cell j and the UE k in cell l with $\mathbf{h}_{lk}^{j}$, it now becomes the canal between AP l and UE k denoted as $\mathbf{h}_{kl}$. The RRH called BS in cellular networks are now called *Access Point* (AP).

4.1.1 User-Centric Dynamic Cooperation Clustering

In order to speak with precision, cell-free mMIMO networks and user-centric cell-free mMIMO networks must be distinguished. In the former case, it is assumed that all UEs are served by all APs. This is not useful in a large network since only a subset of APs standing relatively close to each UEs will experience sufficiently large channel gains to establish fairly good quality communication. Furthermore, this scheme is not scalable since when the number of UEs in the network grows to infinity $K \to \infty$, the computational complexity of the CPU follows this trend. This is why user-centric cell-free mMIMO networks have been defined. In this case, only a fraction of all the APs in the network will serve each UE, as defined in Definition 4.1. An example of such a network is illustrated in Figure 4.1 where each UE is served by the APs belonging to the cluster of its corresponding color.

Definition 4.1. Dynamic cooperation clustering (DCC) defines a subset of APs that are serving a particular UE k. The indices of these APs are in the set $\mathcal{M}_k \subset \{1, ..., L\}$ [3].

For notational convenience, it is useful to define a set of diagonal matrices $\mathbf{D}_{kl} \in \mathbb{C}^{N \times N}$, for $k = 1, ..., K$ and $l = 1, ..., L$. The matrices $\mathbf{D}_{kl}$ associate APs to the UEs with whom they communicate determining which APs communicate with which UEs. They do so by defining themselves as $\mathbf{I}_N$ if AP l can receive/transmit signals from/to UE k and as $\mathbf{0}_{N \times N}$ otherwise. According to the notation of Definition 4.1, it gives

$$\mathbf{D}_{kl} = \begin{cases} \mathbf{I}_N & l \in \mathcal{M}_k \\ \mathbf{0}_{N \times N} & l \notin \mathcal{M}_k \end{cases} \tag{4.1}$$

The original form of the cell-free mMIMO architecture from [39, 40] corresponds to the case where all matrices $\mathbf{D}_{kl} = \mathbf{I}_N$ and means that $\mathcal{M}_k = \{1, ..., L\}$ for $k = 1, ..., K$.

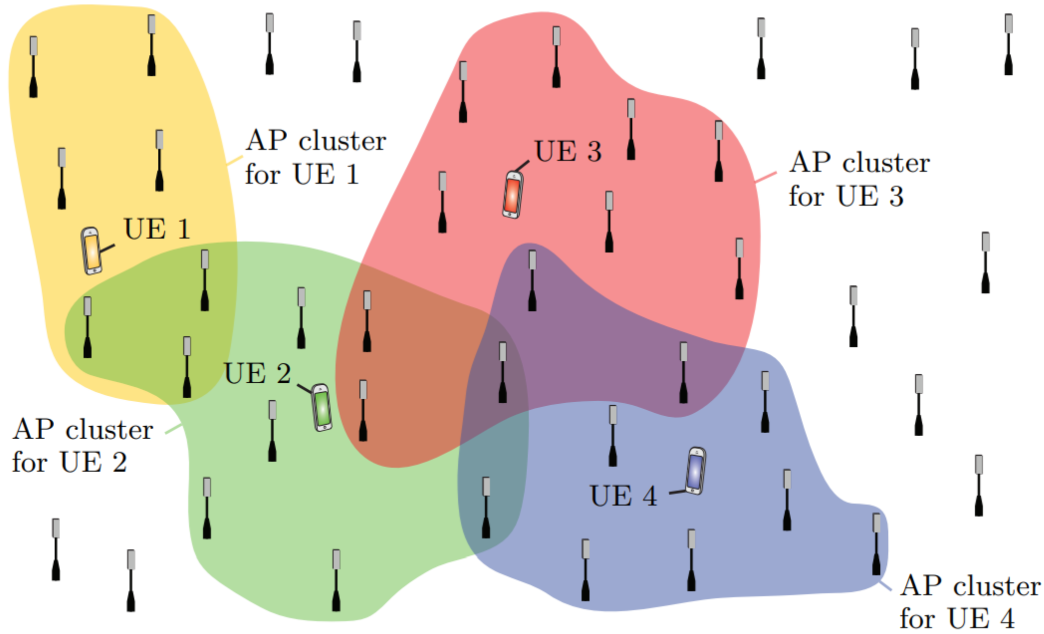

Figure 4.1: Illustration of a DCC setup with 4 clusters (one for each UE). In this user-centric mMIMO network $L >> K$ [3].

In the performance evaluation chapter, the clustering algorithm works as follows. Each AP can serve τ_p (which is the number of orthogonal pilots in the network[1]) different UEs. In order to avoid strong pilot contamination, APs should not serve two UEs sharing the same pilot. Therefore, for each pilot, AP l will select the UE with the strongest channel gain among all the UEs sharing this pilot. This is the way the DCC is constructed in the simulations of Chapter 5. Algorithm 1 describes it in an algorithmic way. The name of the algorithm comes from the fact that the DCC is performerd jointly with the pilot assignement scheme described in Algorithm 2.

4.1.2 Network Topology

In the simulations, the APs are always considered as located 10 meters above the plane to which the UEs belong. The number M of antennas in the entire network is fixed and is equal to $M = 400 = LN$ with L the number of APs and N the number of antennas per AP (which is the same for every AP). The number of APs will be either $L = 400$ or $L = 100$ and therefore the number of antennas per AP will be respectively $N = 1$ or $N = 4$. To remain consistent M will be equal to the

[1]More information about pilot signals is provided in Section 4.1.4

Algorithm 1 Joint AP selection and pilot assignement [3]

Initialization: Set $\mathcal{M}_1 = ... = \mathcal{M}_K = \emptyset$;
for $l = 1, ..., L$ **do**
    for $t = 1, ..., \tau_p$ **do**
        $i \leftarrow \arg \max_{k \in \{1,...,K\}: t_k = t} \beta_{kl}$;
        $\mathcal{M}_i \leftarrow \mathcal{M}_i \cup \{l\}$
    end for
end for
Output: DCCs $\mathcal{M}_1, ..., \mathcal{M}_K$;

number of antennas in the cellular networks used in the simulation.

The network area is a square of dimension 1 km × 1 km (in a wrap-around topology in order to avoid edge effects) in which APs and UEs are deployed randomly. The APs positions follow a uniform distribution

$$[x_l, y_l] \sim \mathcal{U}_{[0,1]} \tag{4.2}$$

The number of UEs is fixed to $K = 40$ and their positions follow the same distribution as the one of the APs. The topology of the network changes in every Monte-Carlo setup (used in the simulation). Each Monte-Carlo setup contains a large number of coherence blocks (and therefore channel realizations).

4.1.3 Channel Modeling

This section describes the channel model used in the simulations of cell-free mMIMO networks. For the same reasons as those mentioned in Section 3.1.2, the channel model used in the simulation of the cell-free networks follows a correlated Rayleigh fading. Multiple measurement campaigns have revealed that using an uncorrelated Rayleigh fading model is practically inadequate, primarily due to the statistical correlation among elements in the channel vector [41]. This phenomenon is called *spatial correlation*. This comes from the fact that certain spatial directions are more likely to establish quality connections between APs and UEs.

Correlated Rayleigh Fading

The correlated Rayleigh fading model finds its suitability in scenarios involving NLoS channels characterized by extensive multipath propagation. The elements of the channel vectors follow a normal distribution and the latter are distributed as

$$\mathbf{h}_{kl} \sim \mathcal{N}_{\mathbb{C}}(\mathbf{0}_N, \mathbf{R}_{kl}) \tag{4.3}$$

where $\mathbf{R}_{kl} \in \mathbb{C}^{N \times N}$ is the correlation matrix. The analytical expression of the (m, ℓ)th element of $\mathbf{R}$ is given in (3.3). The expression of the correlation matrix of $\mathbf{h}_{kl}$ is given by $\mathbb{E}\{\mathbf{h}_{kl}\mathbf{h}_{kl}^{\mathrm{H}}\} = \mathbf{R}_{kl}$. The small-scale fading is modeled by the normal distribution and the large-scale fading by the correlation matrix $\mathbf{R}_{kl}$. These correlation matrices $\mathbf{R}_{kl}$ are considered available at the APs at any time. While the channels between UE k and the N antennas of AP l are correlated, it is assumed $\mathbb{E}\{\mathbf{h}_{kn}\mathbf{h}_{kl}^{\mathrm{H}}\} = \mathbf{0}_{N \times N}$ for $l \neq n$ which means that there is no correlation between the channel vectors of different APs.

Large-Scale Fading Model

The model described in the previous section holds for any fading values but a practical model is needed for the simulations. Cell-free networks are suited for urban environments, intended to operate in area where UEs and APs are densely deployed. UEs are deployed on the ground while APs are standing 10 meters above them. This channel model matches with the one described by the 3GPP Urban Microcell model defined in [42, Table B.1.2.1-1]. This is well-suited for a 2GHz carrier frequency. The channel gains are therefore computed in the simulations (in dB) as

$$\beta_{kl}[\mathrm{dB}] = -30.5 - 36.7 \log_{10}\left(\frac{d_{kl}}{1\mathrm{m}}\right) + F_{kl} \tag{4.4}$$

where d_{kl} [m] is the 3-D distance between AP l and UE k. The shadow fading is modeled by $F_{kl} \sim \mathcal{N}(0, 4^2)$. It is considered that there is some correlation in the shadowing terms of two different UEs that are served by a common AP [42, Table B.1.2.1-4].

$$\mathbb{E}\{F_{kl}F_{ij}\} = \begin{cases} 4^2 2^{-\delta_{ki}/9\mathrm{m}} & l = j \\ 0 & l \neq j \end{cases} \tag{4.5}$$

where δ_{ki} is the distance between UE k and UE i. The shadowing occurring for two different APs is considered as uncorrelated since generally, the distance between two different APs is larger than several meters.

The large-scale fading coefficient β_{kl} in (4.5) are used to compute the spatial correlation matrices $\mathbf{R}_{kl}$. Further information about the way they are computed can be found in [3, Section 2.5.3].

4.1.4 Channel Estimation

According to the block-fading model assumption, in each coherence block, the channel vector $\mathbf{h}_{kl}$ undergoes an independent realization. The channel can be considered as being constant and the same within a coherence block in both uplink and downlink due to the channel reciprocity of physical channels. Therefore, it only needs to be estimated once during the uplink pilot transmission. The channel estimated during uplink pilot transmission will then be used for downlink operations. An illustration of such a coherence block was provided in Figure 3.2.

Let's consider a user-centric cell-free network where a subset of APs (with indices in the set $\mathcal{M}_k \subset \{1, ..., L\}$) are serving UE k. The channel responses between UE k and these APs must be known so that the CPU can define the precoding vectors used in the downlink transmission as explained in Section 4.2. To do so, the CPU will estimate the channel vectors using uplink pilot signals.

As shown in Figure 3.2, τ_p samples are allocated to the transmission of uplink pilot signals. Ideally, each pilot sequence allocated to a particular UE should be orthogonal to the pilot sequences of the other UEs of the network in order to completely avoid pilot contamination (cf. [3, Sec. 4.2.2]). In practice this is something that is not achievable when the number of UEs K is large. Indeed, the pilot sequences are vectors that can contain at most τ_p elements, meaning that a maximum of τ_p mutually orthogonal sequences can be defined. Furthermore τ_p must remain relatively small compared to τ_u in order to maintain a decent data rate during uplink operations. The network can use τ_p pilot sequences $\boldsymbol{\phi}_1, ..., \boldsymbol{\phi}_{\tau_p} \in \mathbb{C}^{\tau_p}$ that are mutually orthogonal and designed to satisfy $||\boldsymbol{\phi}_t||^2 = \tau_p$, for $t = 1, ..., \tau_p$. One option is to use the columns of $\sqrt{\tau_p}\mathbf{I}_{\tau_p}$. What is important for the context of this document is that

$$\boldsymbol{\phi}_{t_1}^{\mathrm{H}}\boldsymbol{\phi}_{t_2} = \begin{cases} \tau_p & t_1 = t_2 \\ 0 & t_1 \neq t_2 \end{cases} \tag{4.6}$$

which allows UE k to suppress interference coming from UEs having a different pilot sequence. As mentioned earlier, in practice several UEs will share the same pilot sequence. The pilot assigned to UE k is designated by the index $t_k \in \{1, ..., \tau_p\}$ which is used to define the set of UEs sharing the same pilot sequence as user k, encompassing user k itself as

$$\mathcal{P}_k = \{i : t_i = t_k, i = 1, ..., K\} \subset \{1, ..., K\} \tag{4.7}$$

The estimation of the channel $\{\mathbf{h}_{kl} : l \in \mathcal{M}_k\}$ is performed at the CPU (since the centralized operations are studied but it could be done at AP l if workinkg in the distributed case) based on $\mathbf{Y}_l^{\text{pilot}} \in \mathbb{C}^{N \times \tau_p}$ which is the pilot received signal at AP l and is given by

$$\mathbf{Y}_l^{\text{pilot}} = \sum_{i=1}^{K} \sqrt{\eta_i}\mathbf{h}_{il}\boldsymbol{\phi}_{t_i}^{\text{T}} + \mathbf{N}_l \tag{4.8}$$

where $\eta_i \geq 0$ is the power of the uplink signal transmitted by UE i and $\mathbf{N}_l \in \mathbb{C}^{N \times \tau_p}$ is the noise at the receiver whose elements are i.i.d. and distributed according to $\mathcal{N}_{\mathbb{C}}(0, \sigma_{\text{ul}}^2)$

MMSE Channel Estimation

In order to estimate $\mathbf{h}_{kl}$, the CPU will cancel inter-user interference by using orthogonal pilots. To do so, multiplying the $\mathbf{Y}_l^{\text{pilot}}$ with the normalized conjugate of $\boldsymbol{\phi}_{t_k}$ which is the associated pilot. This yields $\mathbf{y}_{t_k l}^{\text{pilot}} = \mathbf{Y}_l^{\text{pilot}}\boldsymbol{\phi}_{t_k}^*/\sqrt{\tau_p} \in \mathbb{C}^N$ given by

$$\begin{aligned}\mathbf{y}_{t_k l}^{\text{pilot}} &= \sum_{i=1}^{K} \frac{\sqrt{\eta_i}}{\sqrt{\tau_p}}\mathbf{h}_{il}\boldsymbol{\phi}_{t_k}^{\text{T}}\boldsymbol{\phi}_{t_k}^* + \frac{1}{\sqrt{\tau_p}}\mathbf{N}_l\boldsymbol{\phi}_{t_k}^* \\ &= \underbrace{\sqrt{\eta_k\tau_p}\mathbf{h}_{kl}}_{\text{Desired part}} + \underbrace{\sum_{i \in \mathcal{P}_k \setminus \{k\}} \sqrt{\eta_i\tau_p}\mathbf{h}_{il}}_{\text{Interference}} + \underbrace{\mathbf{n}_{t_k l}}_{\text{Noise}}\end{aligned} \tag{4.9}$$

where the first term is the desired channel $\mathbf{h}_{kl}$ scaled by $\sqrt{\eta_k\tau_p}$ (the square root of the total pilot power $||\sqrt{\eta_k}\boldsymbol{\phi}_{t_k}||^2 = \eta_k\tau_p$). The second term comes from the interference generated by the UEs sharing the same pilot sequence and the third term is the noise $\mathbf{n}_{t_k l} = \frac{1}{\sqrt{\tau_p}}\mathbf{N}_l\boldsymbol{\phi}_{t_k}^* \sim \mathcal{N}_{\mathbb{C}}(\mathbf{0}_N, \sigma_{\text{ul}}^2\mathbf{I}_N)$. The processed pilot signal $\mathbf{y}_{t_k l}^{\text{pilot}}$ is used to compute the channel estimates as represented in (4.10).

Theorem 4.1. The CPU estimates the channel vector $\mathbf{h}_{kl}$ based on $\mathbf{y}_{t_k l}^{\text{pilot}}$ using the following MMSE estimator

$$\widehat{\mathbf{h}}_{kl} = \sqrt{\eta_k\tau_p}\mathbf{R}_{kl}\boldsymbol{\Psi}_{t_k l}^{-1}\mathbf{y}_{t_k l}^{\text{pilot}} \tag{4.10}$$

where

$$\boldsymbol{\Psi}_{t_k l} = \mathbb{E}\left\{\mathbf{y}_{t_k l}^{\text{pilot}}(\mathbf{y}_{t_k l}^{\text{pilot}})^{\text{H}}\right\} = \sum_{i \in \mathcal{P}_k} \eta_i\tau_p\mathbf{R}_{il} + \sigma_{\text{ul}}^2\mathbf{I}_N \tag{4.11}$$

is the correlation matrix of the processed pilot signal in (4.9). (4.12) and (4.13) give respectively the distributions of the channel estimate and of the estimation error. These two variables are independently and randomly distributed. The estimation error is defined as $\widetilde{\mathbf{h}}_{kl} = \mathbf{h}_{kl} - \widehat{\mathbf{h}}_{kl}$.

$$\widehat{\mathbf{h}}_{kl} \sim \mathcal{N}_{\mathbb{C}}\left(\mathbf{0}_N, \eta_k \tau_p \mathbf{R}_{kl} \mathbf{\Psi}_{t_k l}^{-1} \mathbf{R}_{kl}\right) \tag{4.12}$$

$$\widetilde{\mathbf{h}}_{kl} \sim \mathcal{N}_{\mathbb{C}}(\mathbf{0}_N, \mathbf{C}_{kl}) \tag{4.13}$$

where

$$\mathbf{C}_{kl} = \mathbb{E}\left\{\widetilde{\mathbf{h}}_{kl}\widetilde{\mathbf{h}}_{kl}^{\mathrm{H}}\right\} = \mathbf{R}_{kl} - \eta_k \tau_p \mathbf{R}_{kl} \mathbf{\Psi}_{t_k l}^{-1} \mathbf{R}_{kl} \tag{4.14}$$

is the error correlation matrix.

The theorem can be found in [3, Section 4.2].

4.2 Downlink Operation

In the downlink operation, AP l transmit a signal denoted by $\mathbf{x}_l \in \mathbb{C}^N$. After propagation through the downlink channel $\mathbf{h}_{kl}^{\mathrm{H}}$, UE k receives the following signal

$$y_k^{\mathrm{dl}} = \sum_{l=1}^{L} \mathbf{h}_{kl}^{\mathrm{H}} \mathbf{x}_l + n_k \tag{4.15}$$

wher $n_k \sim \mathcal{N}_{\mathbb{C}}(0, \sigma_{\mathrm{dl}}^2)$ is the noise. The downlink channel is represented by $\mathbf{h}_{kl}^{\mathrm{H}}$. As explained is Section 3.2, the complex conjugate in $\mathbf{h}_{kl}^{\mathrm{H}}$ is used to simplify the notation even if in the simulation it is a transpose that is performed.

$\varsigma_i \in \mathbb{C}$ is the data signal that the serving APs of UE i will jointly transmit. Its power is unitary thus $\mathbb{E}\{|\varsigma_i|^2\} = 1$. The average power of the transmitted data signal $\mathbf{x}_l$ (defined in (4.16)) will be determined by the average squared norm $\mathbb{E}\{||\mathbf{w}_{il}||^2\}$ ($\mathbf{w}_{il}$ is defined here after) of the precoding vector. When transmitting, each AP sums up the data signals intended for every UEs that it serves. This precoded superposition of data signals is given by

$$\mathbf{x}_l = \sum_{i=1}^{K} \mathbf{D}_{il} \mathbf{w}_{il} \varsigma_i \tag{4.16}$$

where $\mathbf{w}_{il} \in \mathbb{C}^N$ is any precoding vector. Its direction $\mathbf{w}_{il}/||\mathbf{w}_{il}||$ determines the spatial directivity of $\mathbf{x}_l$.

As for the uplink, the *effective transmit precoding vector* can be defined as

$$\mathbf{D}_{il}\mathbf{w}_{il} = \begin{cases} \mathbf{w}_{il} & l \in \mathcal{M}_i \\ \mathbf{0}_N & l \notin \mathcal{M}_i \end{cases} \tag{4.17}$$

since $\mathbf{D}_{il} = \mathbf{0}_{N\times N}$ implies $\mathbf{D}_{il}\mathbf{w}_{il} = \mathbf{0}_N$. This allows each AP to define precoding vectors only for the subset of UEs that it serves. That is to say when $\mathbf{D}_{il} \neq \mathbf{0}_{N\times N}$.

By substituting the transmitted signal in (4.16) into (4.15) and by extracting the index $i = k$ from the sum, the received downlink signal at UE k becomes

$$\begin{aligned} y_k^{\text{dl}} &= \sum_{l=1}^{L} \mathbf{h}_{kl}^{\text{H}} \left(\sum_{i=1}^{K} \mathbf{D}_{il}\mathbf{w}_{il}\varsigma_i \right) + n_k \\ &= \sum_{l=1}^{L} \mathbf{h}_{kl}^{\text{H}} \mathbf{D}_{kl}\mathbf{w}_{kl}\varsigma_k + \sum_{\substack{i=1 \\ i\neq k}}^{K} \sum_{l=1}^{L} \mathbf{h}_{kl}^{H} \mathbf{D}_{il}\mathbf{w}_{il}\varsigma_i + n_k \end{aligned} \tag{4.18}$$

(4.18) can be divided into three terms. They are, in order, the desired signal, the interference coming from the signals intended for the other UEs and the noise. This expression holds for any precoding vector $\mathbf{w}_{il}$. The data detection on the UE side in the downlink is performed using SDMA.

In the centralized downlink, the APs only act as RRH that transmit signals sended by the CPU through fronthaul links. The CPU is responsible for the data encoding and the generation of the precoding vectors $\mathbf{w}_{il} \in \mathbb{C}^N$ as illustrated in Figure 4.2. The collective precoding vectors $\{\mathbf{D}_i\mathbf{w}_i : i = 1, ..., K\}$ are computed by the CPU using MMSE estimates for all the K UEs in the network. It will also generate a signal $\mathbf{x}_l$, developed in (4.16), for each AP, where $\{\varsigma_i : i = 1, ..., K\}$ is the downlink data. The downlink channel vectors $\mathbf{h}_{kl}^{\text{H}}$ in (4.18) are, for their part, considered as known by the UEs. Only the case where the UEs know the CSI perfectly is studied in this document.

4.2.1 Precoding Vectors

The SE (resp. EMF exposure) expression presented in Section 4.2.2 (resp. Section 4.2.3) holds for any centralized precoding vector.

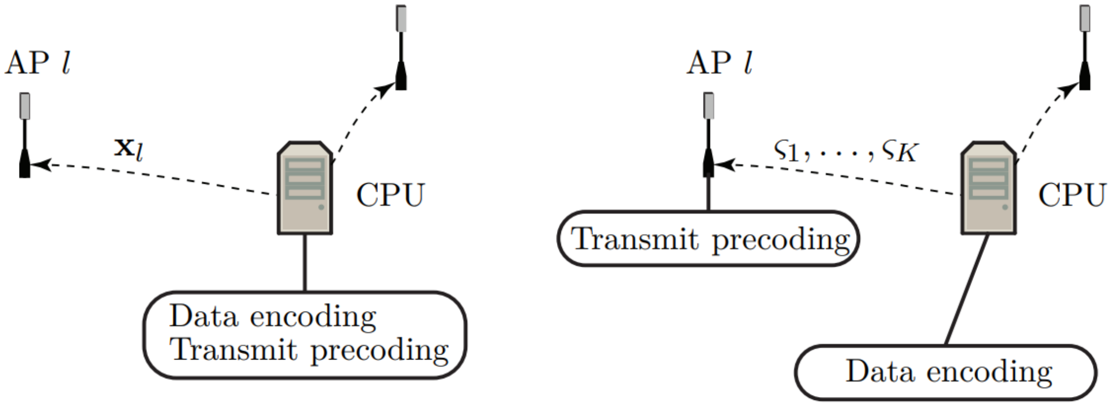

(a) Centralized operation (b) Distributed operation

Figure 4.2: Comparison between the cell-free centralized and distributed operation. In the centralized case, APs are only acting as RRH while the CPU is responsible of all the computation. In the distributed case, the CPU is only responsible of the data encoding while the APs compute their own transmit precoding vectors [3]. Only the centralized case is considered in this document.

$$\mathbf{w}_k = \sqrt{\rho_k}\frac{\bar{\mathbf{w}}_k}{\sqrt{\mathbb{E}\{||\bar{\mathbf{w}}_k||^2\}}} \tag{4.19}$$

The denominator in (4.19) ensures that

$$\mathbb{E}\{||\mathbf{w}_k||^2\} = \rho_k \tag{4.20}$$

The centralized precoding vectors $\bar{\mathbf{w}}_k$, used in this document, are presented below.

MMSE

The MMSE precoding which minimizes the mean squared error between the signal received by all UEs and their data signals.

$$\bar{\mathbf{w}}_k^{\mathrm{MMSE}} = p_k \left(\sum_{i=1}^{K} p_i \mathbf{D}_k (\widehat{\mathbf{h}}_i \widehat{\mathbf{h}}_i^{\mathrm{H}} + \mathbf{C}_i) \mathbf{D}_k + \sigma_{\mathrm{ul}}^2 \mathbf{I}_{LN} \right)^{-1} \mathbf{D}_k \widehat{\mathbf{h}}_k \tag{4.21}$$

where p_k is the uplink transmitted power by UE k, $\mathbf{D}_k = \mathrm{diag}(\mathbf{D}_{k1}, ..., \mathbf{D}_{kL}) \in \mathbb{C}^{LN}$ and $\widehat{\mathbf{h}}_k = \left[\widehat{\mathbf{h}}_{k1}, ..., \widehat{\mathbf{h}}_{kL}\right]^{\mathrm{T}} \in \mathbb{C}^{LN}$.

P-MMSE

Starting from (4.21) and by considering that only a fraction of UEs (i.e. all the UEs having a least one common AP with UE k) produce significant interference, it gives

$$\bar{\mathbf{w}}_k^{\text{P-MMSE}} = p_k \left(\sum_{i \in \mathcal{S}_k} p_i \mathbf{D}_k \widehat{\mathbf{h}}_i \widehat{\mathbf{h}}_i^{\text{H}} \mathbf{D}_k + \mathbf{Z}_{\mathcal{S}_k} + \sigma_{\text{ul}}^2 \mathbf{I}_{LN} \right)^{-1} \mathbf{D}_k \widehat{\mathbf{h}}_k \tag{4.22}$$

where

$$\mathcal{S}_k = \{ i : \mathbf{D}_k \mathbf{D}_i \neq \mathbf{0}_{LN \times LN} \} \tag{4.23}$$

is the set of UEs served by at least one AP that also serves UE k, including itself and

$$\mathbf{Z}_{\mathcal{S}_k} = \sum_{i \in \mathcal{S}_k} p_i \mathbf{D}_k \mathbf{C}_i \mathbf{D}_k \tag{4.24}$$

P-MMSE reduces the calculation complexity compared to MMSE since the size of the matrix to be inverted is reduced.

P-RZF

Calculation complexity can be further reduced by taking (4.22) and considering that the estimation error correlation matrix $\mathbf{Z}_{\mathcal{S}_k}$ can be neglected. This leads to

$$\bar{\mathbf{w}}_k^{\text{P-RZF}} = p_k \left(\sum_{i \in \mathcal{S}_k} p_i \mathbf{D}_k \widehat{\mathbf{h}}_i \widehat{\mathbf{h}}_i^{\text{H}} \mathbf{D}_k + \sigma_{\text{ul}}^2 \mathbf{I}_{LN} \right)^{-1} \mathbf{D}_k \widehat{\mathbf{h}}_k \tag{4.25}$$

In Chapter 5, numerical results will show that the performance losses of these two last precoding schemes are really small.

4.2.2 Spectral Efficiency

To obtain an expression for the spectral efficiency that a UE in the network can achieve and that is applicable for any precoding, let's start by defining the received signal in (4.26). It can be divided into three terms :

$$y_k^{\mathrm{dl}} = \underbrace{\mathbf{h}_k^{\mathrm{H}} \mathbf{D}_k \mathbf{w}_k \varsigma_k}_{\text{Desired signal}} + \underbrace{\sum_{\substack{i=1 \\ i \neq k}}^{K} \mathbf{h}_k^{\mathrm{H}} \mathbf{D}_i \mathbf{w}_i \varsigma_i}_{\text{Inter-user interference}} + \underbrace{n_k}_{\text{Noise}} \tag{4.26}$$

The desired signal is the term from which the UE k wants to extract the data. It corresponds to the combination of signals intended for UE k and sent by every AP of the network (recall that this is the general model in which it is considered that every AP serves every UE). The second term includes the signals intended for the other UEs of the network. The third term is the noise. The precoding vector is also known by the CPU since it computes it as well as the partial MMSE estimate of the channel. In order to remain consistent with the cellular networks, it is assumed, in this document, that the UEs have perfect knowledge of the CSI in downlink. Therefore, the MMSE estimation of the channel described in Section 4.1.4 is only used by the APs to define the precoding vectors $\mathbf{w}_{il}$.

Theorem 4.2. The expression of SE achievable by UE k in downlink with centralized operation when considering that the UE have knowledge of the perfect CSI is

$$\mathrm{SE}_k^{(\mathrm{dl,c})} = \frac{\tau_d}{\tau_c} \mathbb{E}\left\{ \log_2 \left(1 + \mathrm{SINR}_k^{(\mathrm{dl,c})} \right) \right\} \quad \text{bit/s/Hz} \tag{4.27}$$

where the instantaneous effective SINR is

$$\mathrm{SINR}_k^{(\mathrm{dl,c})} = \frac{\left| \sum_{l=1}^{L} \mathbf{h}_{kl}^{\mathrm{H}} \mathbf{D}_{kl} \mathbf{w}_{kl} \right|^2}{\sum_{\substack{i=1 \\ i \neq k}}^{K} \left| \sum_{l=1}^{L} \mathbf{h}_{kl}^{\mathrm{H}} \mathbf{D}_{il} \mathbf{w}_{il} \right|^2 + \sigma_{\mathrm{dl}}^2} \tag{4.28}$$

4.2.3 EMF Exposure

Starting from (4.28), the EMF exposure of UE k is derived in (4.29)

$$\xi_k = \frac{4\pi}{\lambda^2} \sum_{i=1}^{K} \left| \sum_{l=1}^{L} \mathbf{h}_{kl}^{\mathrm{H}} \mathbf{D}_{il} \mathbf{w}_{il} \right|^2 \tag{4.29}$$

This expression takes into account the contribution of the desired and interfering signals. $\lambda = c/\kappa$ is the carrier wavelength, with $\kappa = 2$ GHz the carrier frequency and c the speed of light in vacuum.

5

Simulation Results

In order to compare the performances of the user-centric cell-free mMIMO with the one of well known cellular mMIMO networks, this section defines network setups that have been used to simulate the two networks. They rely on the mathematics developed in Chapters 3 and 4.

Making a fair comparison between the two kinds of network can be complicated. In order to remain as consistent as possible, the total number of antennas in both networks ($M = \sum_{l=1}^{L} N_l$ in the cellular case and $M = LN$ in the cell-free case) is fixed to 400. In the cellular network, the number of BSs L is always fixed to 4 with $M_j = 100\ \forall j$ (the number of antennas per BSs) and in the cell-free case, the number of APs can either be $L = 400$ or $L = 100$. In the former case, each AP contains $N = 1$ antenna while in the second $N = 4$. BSs are always placed at the center of their cell while the APs are randomly deployed through the network area according to (4.2). The operating carrier frequency of both networks is $\kappa = 2$ GHz and the bandwidth $B = 20$ MHz. The coverage area is a 1 km $\times$ 1 km square using a wrap-around topology in both networks. The wrap-around is used to simulate a large network deployment.

The large-scale fading coefficient (channel gain) are computed based on (3.4) and (4.4). For the cellular setup, two different large-scale fading model will be used. Indeed, one setup makes use of parameters that matches with those of a macro-cell cellular network in an urban area[1] as described in Section 3.1.2. The other model

[1]These parameters come from [9] and match with the NLoS macro-cell 3GPP model for 2 GHz carriers, described in [43, Table A.2.1.1.2-3]

uses the same parameters as those used in the cell-free simulations, they match with a small cells network. The different scenarios are spelled out respectively as *Macro-cell* and *Micro-cell* in the legends of the figures that follow.

One thing that can be difficult to simulate in both networks in order to remain consistent is the downlink power allocation. To limit its impact, both setups use two power allocation heuristics. On the cellular side, each BS allows 100 mW to every UE it serves. On the cell-free side, each AP has a maximum downlink power of $\rho_{\max} = 400$ mW that it has to divide between all the UEs it serves as follows :

$$\rho_k = \rho_{\max} \frac{\left(\sum_{l \in \mathcal{M}_k} \beta_{kl} \right)^{-\frac{1}{2}} \omega_k^{-\frac{1}{2}}}{\max_{\ell \in \mathcal{M}_k} \sum_{i \in \mathcal{D}_\ell} \left(\sum_{l \in \mathcal{M}_i} \beta_{il} \right)^{-\frac{1}{2}} \omega_i^{\frac{1}{2}}} \tag{5.1}$$

where $\mathcal{D}_l$ is the set of UEs served by AP l and

$$\omega_k = \max_{\ell \in \mathcal{M}_k} \mathbb{E} \left\{ ||\bar{\mathbf{w}}'_{k\ell}||^2 \right\} \beta_{kl} \tag{5.2}$$

where $\bar{\mathbf{w}}'_{k\ell}$ is equal to $\frac{\bar{\mathbf{w}}_k}{\sqrt{\mathbb{E}||\bar{\mathbf{w}}_k||^2}}$ from (4.19). Basically, this algorithm allows UEs with a larger total channel gain to receive more power [3, Section 7.2.2]. In this setup, the power allocated to each UE can vary over time. The distribution of the power allocated per UE is illustrated in Figure 5.1 for different precoding schemes when $L = 400$ and $N = 1$. On average, for a UE k, the sum of the power allocated by all the APs serving it is equal to $\bar{\rho}_k = 102.06$ mW when using the MMSE precoding scheme. This means that, on average, the same power (to within a few mW) can be allocated to each user in both types of networks. The effect of the power allocation is analyzed in Section 5.1.4.

The main objective of these simulations is not really to obtain exact values of SE or EMF exposure. Indeed the models are simple and considering the several assumptions described earlier, the resulting data may differ slightly from real values. The aim is rather to, compare the performance of both networks and to discuss the potential feasibility of user-centric cell-free networks.

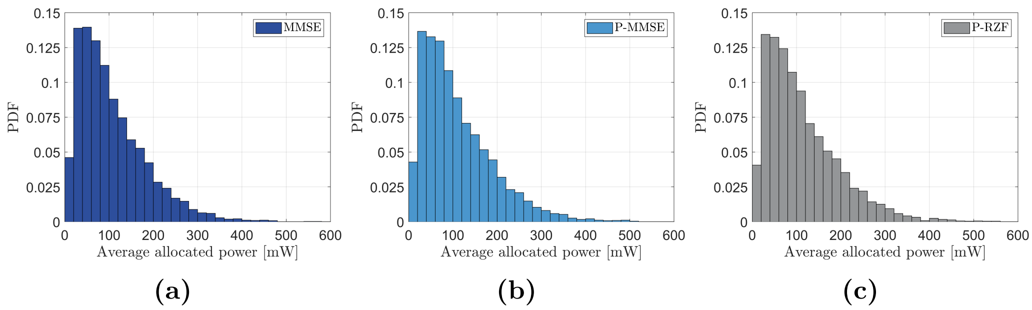

Figure 5.1: PDF of the average allocated downlink power $\mathbb{E}\{||\mathbf{w}_{il}||^2\}$ in cell-free networks for three precoding schemes in the case where $L = 400$ and $N = 1$. The expectation is with respect to the channel realizations. The average allocated power per UE using the MMSE precoding scheme is equal to $\bar{\rho}_k = 102.06$ mW.

Important note : As mentioned in the acknowledgements section, the computational resources have been provided by the supercomputing facilities of the Université catholique de Louvain (CISM/UCL) and the Consortium des Équipements de Calcul Intensif en Fédération Wallonie Bruxelles (CÉCI). It has mainly been used for the simulations of the cell-free networks due to their heavy computational complexity. The simulation code supplied jointly with [9] and [3] have served as a base material to perform respectively the cellular simulations[a] and the cell-free ones[b].

[a]Code available here : `https://massivemimobook.com/wp/`
[b]Code available here : `https://github.com/emilbjornson/cell-free-book`

5.1 Numerical results

The simulations have been performed using Monte Carlo methodologies. The source of randomness in each Monte Carlo setup comes from the position of the UEs and the APs that are regenerated in each one of them as well a the shadow fading realizations. The parameters used during the simulations are detailed in Table 5.1 for the cellular setups. *Macro-cell* and *Micro-cell* indicates the type of channel model parameters (i.e. large-scale fading coefficients and shadow fading standard deviation, cf. Table 5.1) that are used. These notations are repeated in the legends of the following figures. The parameters of the user-centric cell-free setups are detailed in Table 5.2. Different precoding schemes are compared on the following figures. For cellular networks : M-MMSE, S-MMSE, RZF and MR[2] while

[2]The cellular precoding vectors have been defined in Section 3.2.1

Parameter	Value
Network layout	Square pattern (wrap-around)
Number of cells	$L = 4$
Cell area	0.5 km $\times$ 0.5 km
Number of antennas per BS	$N_j = 100\ \forall j$
Numbers of UEs per cell	$K_j = 10\ \forall j$
Channel gain at 1 km (Macro-cell)	$\Upsilon = -148.1$ dB
Channel gain at 1 km (Micro-cell)	$\Upsilon = -140.6$ dB
Pathloss exponent (Macro-cell)	$\alpha = 3.76$
Pathloss exponent (Micro-cell)	$\alpha = 3.67$
Shadow fading (std) (Macro-cell)	$\sigma_{\text{sf}} = 10$
Shadow fading (std) (Micro-cell)	$\sigma_{\text{sf}} = 4$
Bandwidth	$B = 20$ MHz
Receiver noise power	-94 dBm
Downlink transmit power per UE	100 mW
Samples per coherence block	$\tau_c = 200$
Pilot reuse factor	$f = 1$
Number of uplink pilot sequences	$\tau_p = fK_j = 10$

Table 5.1: System parameters used for the simulation of the cellular mMIMO networks. The cells are deployed on a grid of 2 $\times$ 2 cells. Parameters are extrated from [9].

for the cell-free networks : MMSE, P-MMSE and P-RZF[3].

5.1.1 Performance metrics

This section provides an overview of the statistical performance metrics used to compare cellular and cell-free networks.

- The *probability density function* (PDF) $f_{\text{SE}}(T)$ which expresses the likelihood of a random variable taking a value within a specific range. It will be used to illustrates the distribution of the SE and the EMF exposure (in this last case SE is replaced by ξ and T by T').

- The *complementary cumulative distribution function* (CCDF)

$$\bar{F}_{\text{SE}}(T) = P\Big[\text{SE} > T\Big] = 1 - F_{\text{SE}}(T) \tag{5.3}$$

[3]The cell-free precoding vectors have been defined in Section 4.2.1

Parameter	Value
Network layout	Random deployment (wrap-around)
Number of APs	$L = 400$ or $L = 100$
Network area	1 km $\times$ 1 km
Number of antennas per AP	$N = 1$ or $N = 4$
Number of total antennas	$M = LN = 400$
Channel gain at 1 km	$\Upsilon = -140.6$ dB
Pathloss exponent	$\alpha = 3.67$
Shadow fading (standard deviation)	$\sigma_{\text{sf}} = 4$
Bandwidth	$B = 20$ MHz
Receiver noise power	-94 dBm
Maximum downlink transmit power per AP	400 mW
Samples per coherence block	$\tau_c = 200$
Height difference between AP and UE	10 m

Table 5.2: System parameters used for the simulation of the user-centric cell-Free mMIMO networks. Parameters are extrated from [3].

with $F_{\text{SE}}(T)$ being a CDF. The CCDF is used to depict the probability that the SE or the EMF exposure (in that case, SE becomes ξ and T, T') of a particular UE are greater than a certain value T.

- The *conditional complementary cumulative distribution function* also called conditional CCDF

$$\bar{F}_{\text{SE}|\xi}(T|T') = P\Big[\text{SE} > T|\xi \leq T'\Big] \tag{5.4}$$

which depicts the probability that the SE of a UE is greater than a value T knowing that its EMF exposure ξ is lower than a given threshold T'.

- The *joint complementary cumulative distribution function* (or joint CCDF)

$$\bar{F}_{\text{SE},\xi}(T, T') = P\Big[\text{SE} > T, \xi \leq T'\Big] \tag{5.5}$$

illustrating, in a bidimensional way, the probability, for a UE, of achieving a certain SE T while remaining below a certain EMF exposure value T'.

- The *meta distribution*

$$\mathcal{F}_{\mathrm{SINR}}(s,T) = P\Big[P\Big[\mathrm{SINR} > T|[x_k, y_k]\Big] > s\Big] \tag{5.6}$$

$$\mathcal{F}_{\xi}(s,T') = P\Big[P\Big[\xi < T'|[x_k, y_k]\Big] > s\Big] \tag{5.7}$$

corresponds to the CCDF of the coverage probability (resp. EMF exposure) for a UE at a particular position $[x_k, y_k]$ in the network. It is important to notice that the inequalities in (5.6) and (5.7) have opposite signs.

5.1.2 Spectral Efficiency

Figures 5.2 and 5.3 illustrate respectively the CDF and the PDF of the SE for cellular (a) and cell-free networks (b). Figure 5.2a shows that using the *Micro-cell* parameters instead of the *Macro-cell* ones makes no major differences but *Mirco-cell* simulations are slightly better and this is due to the fact that the variance of the shadowing σ_{sf} is smaller in that case.

The precoding scheme that offers the best performance in cellular is M-MMSE. This scheme, however, requires high computational complexity since it takes into account the interfering signals coming from all the other cells and has to compute the channel vectors between the considered BS and all the UEs in the network. S-MMSE, for its part only considers the interference coming from the UEs in the considered cell as well as the channels between them. RZF is achieved by neglecting the channel and error correlation matrices. The performances of the last two precoding schemes are really close to the one of the M-MMSE. The MR precoding offers for its part the lowest SE.

Figure 5.2b illustrates the CDF of the SE for three different precoding schemes and two different cases ($L = 400$, $N = 1$ and $L = 100$, $N = 4$) in cell-free networks. MMSE precoding scheme takes into account the interference coming from all the UEs which makes it a non-scalable scheme. The P-MMSE makes the hypothesis that only a fraction of UEs produces significant interference, and only UEs who have at least one AP in common are considered when calculating precoding. RZF is achieved by considering that there is no error in the uplink channel estimation and therefore that the error correlation matrices $\mathbf{C}_k$ are negligible. The two last schemes are scalable and as illustrated in Figure 5.2b the difference between the performances provided by all the schemes are negligible.

It is, however, interesting to note that the case where there are more APs with less antennas in the network provides a better SE than the case with $L = 100$. Indeed

Precoding	SE [bits/s/Hz]		EMF exposure [dB(mW/m^2)]	
	Mean	Variance	Mean	Variance
M-MMSE (Macro-cell)	5.381	8.243	-14.860	88.818
S-MMSE (Macro-cell)	4.837	7.748	-14.554	87.602
MR (Macro-cell)	2.750	1.0936	-13.171	89.170
RZF (Macro-cell)	4.778	7.517	-14.256	87.883
M-MMSE (Micro-cell)	5.807	4.953	-12.342	49.210
S-MMSE (Micro-cell)	4.975	5.816	-11.673	47.0749
MR (Micro-cell)	2.855	0.933	-10.261	48.193
RZF (Micro-cell)	4.810	5.560	-11.353	47.000

Table 5.3: First and second order moments of the SE and of the EMF exposure in cellular networks for different precoding scheme and channel model parameters.

the curves for $L = 400$ are shifted to the right. Spread out the APs allows a better *macro-diversity gain*.

By comparing Figures 5.2a and 5.2b one can realize that on average, the cell-free networks offer better performances, in term of SE, than the cellular ones. This is however not the case in the lower tail of the curves (around a CDF value of 0.05) where the values of SE are greater in cellular. It depicts the fact that cellular networks can offer to a few UEs very good performances (even better than in cell-free) but also very poor performance to a few others. This last case is illustrated in the upper tail of Figure 5.2a (around a CDF value of 0.9).

The fact that cell-free networks should provide a more uniform coverage might be clearer by looking at the PDF illustrated in Figure 5.3. Indeed, in addition to the fact that the mean values of the SE are greater in cell-free, the variances are also much smaller than in the cellular case. As a reminder, the main aim of the cell-free networks is to offer the most uniform coverage possible in order to enable the mass deployment of interconnected objects. Values of the moments of the SE of order 1 (mean) and 2 (variance) are summarized in Table 5.3 for cellular networks and in Table 5.4 for cell-free networks.

5.1.3 EMF Exposure

Figure 5.4 illustrates the CCDF of the EMF exposure in cellular and cell-free networks in term of IPD [dB(mW/m^2)]. In Figure 5.4a one can see that when using *Micro-cell* channel parameters, the exposure is slightly greater than when using *Macro-cell* parameters. This is due to the fact that there is less shadowing in the former case and therefore there is less shielding provided by obstacles. The

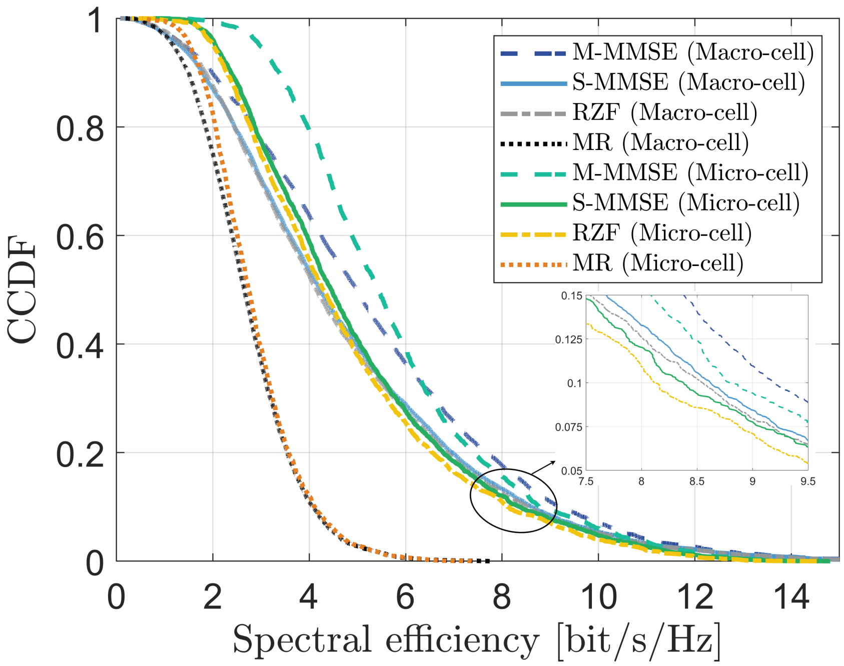

(a) Cellular

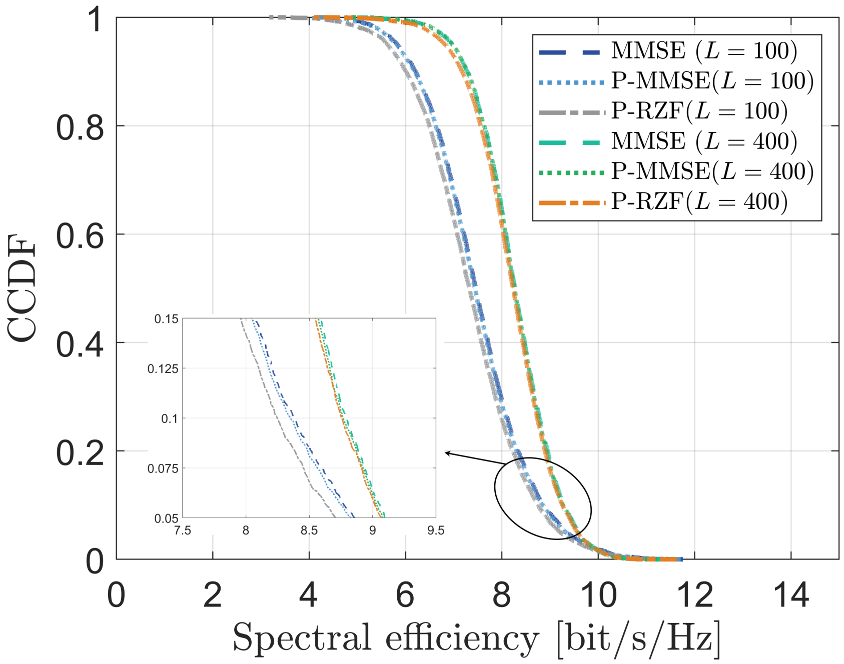

(b) Cell-free

Figure 5.2: CCDF of the downlink spectral efficiency in a cellular mMIMO network (a) and in a user-centric cell-free mMIMO network (b). Both simulations have been performed using perfect CSI on the UE side. The other parameters can be found in Table 5.1 for (a) and in Table 5.2 for (b).

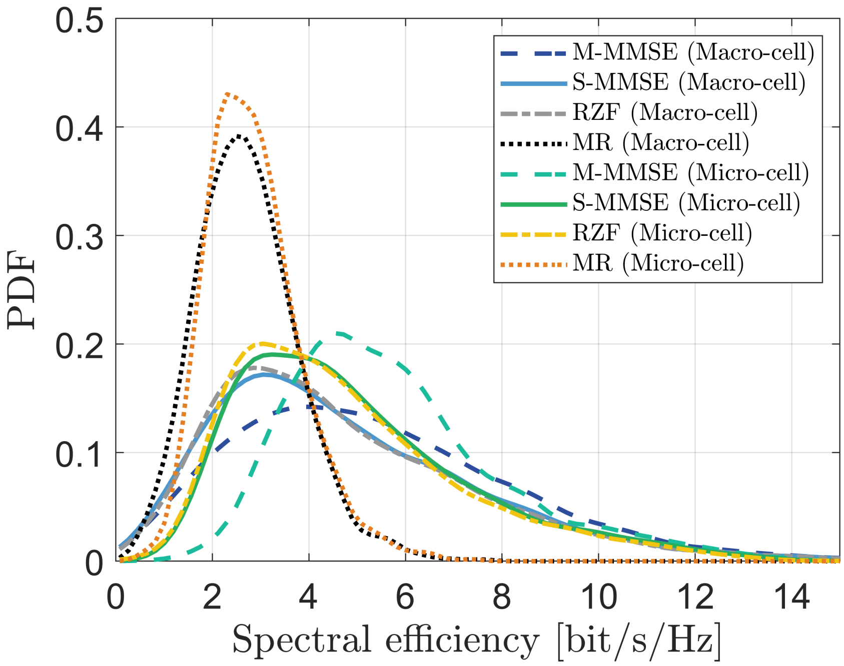

(a) Cellular

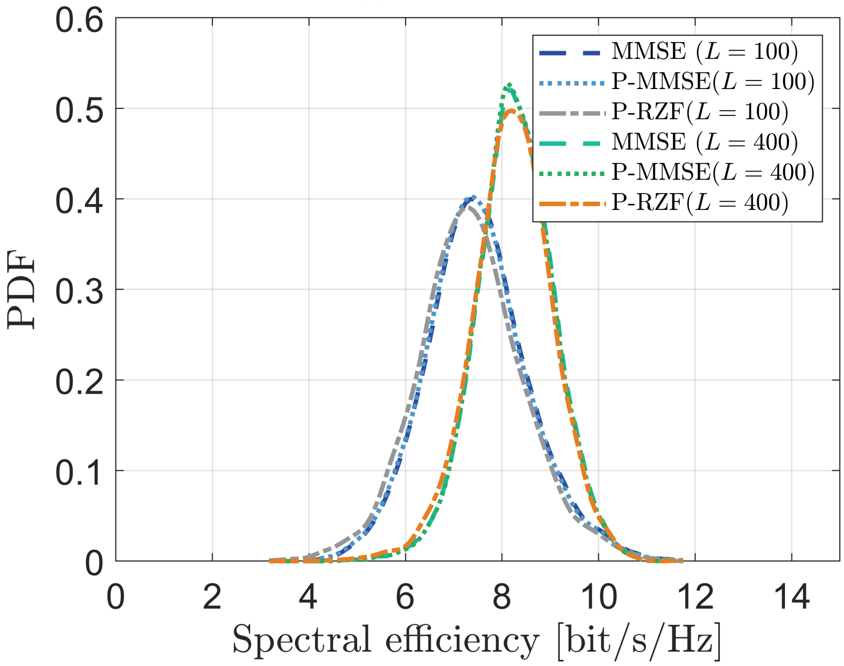

(b) Cell-free

Figure 5.3: PDF of the downlink spectral efficiency in a cellular mMIMO network (a) and in a user-centric cell-free mMIMO network (b). Both simulations have been performed using perfect CSI on the UE side. The other parameters can be found in Table 5.1 for (a) and in Table 5.2 for (b).

Precoding	SE [bits/s/Hz]		EMF exposure [dB(mW/m^2)]	
	Mean	Variance	Mean	Variance
MMSE ($L = 100$)	7.508	1.130	-4.983	9.871
P-MMSE ($L = 100$)	7.484	1.126	-4.871	9.701
P-RZF ($L = 100$)	7.357	1.206	-4.424	9.736
MMSE ($L = 400$)	8.277	0.651	0.270	4.467
P-MMSE ($L = 400$)	8.266	0.636	0.421	4.296
P-RZF ($L = 400$)	8.216	0.708	0.494	4.299

Table 5.4: First and second order moments of the SE and of the EMF exposure in cell-free networks for different precoding scheme and network deployment

difference between the precoding schemes is negligible. On average, a UE will be more exposed to EMF in a cell-free network. This is illustrated more clearly in Figure 5.5. The EMF exposure is a random variable and its variance is for its part much lower in cell-free. The probability that a UE is exposed to a high quantity of EMF is lower than in cellular networks.

In Figure 5.4b the exposure is greater when using a larger number of APs since on average the distance between the UEs and APs is smaller and therefore the signals strength is less attenuated.

In general, larger distances in the cellular case leads to lower EMF exposure values than in cell-free networks due to the high propagation losses that appear in downlink. This is however not true for the lower 5% likely IPD which corresponds to UEs close to a BS.

Figures illustrating the CCDF and PDF of the SE and EMF exposure use multiple precoding schemes in different scenarios. For the figures that follow them, only the M-MMSE precoding scheme is used for the cellular simulations. The *macro-cell* channel parameters is used since they best model this type of network. In cell-free, only the case where $L = 400$ and $N = 1$, using the MMSE precoding is retained. These two scenarios are studied since they provide the best performances in terms of SE.

Figure 5.6 illustrates the conditional CCDF and PDF for cellular and cell-free networks. The conditional CCDF gives the probability of coverage (in terms of SE) that is achievable for a given maximum EMF exposure value. The case where $\xi = 33$ dB(mW/m^2) matches with the EMF exposure boundary (for a carrier frequency of 2.1 GHz) set up by the Walloon region (different limits are summarized in Table 2.1). The other EMF exposure thresholds have been chosen arbitrarily. In cell-free, the maximum EMF exposure that a UE can experience (in the context of these

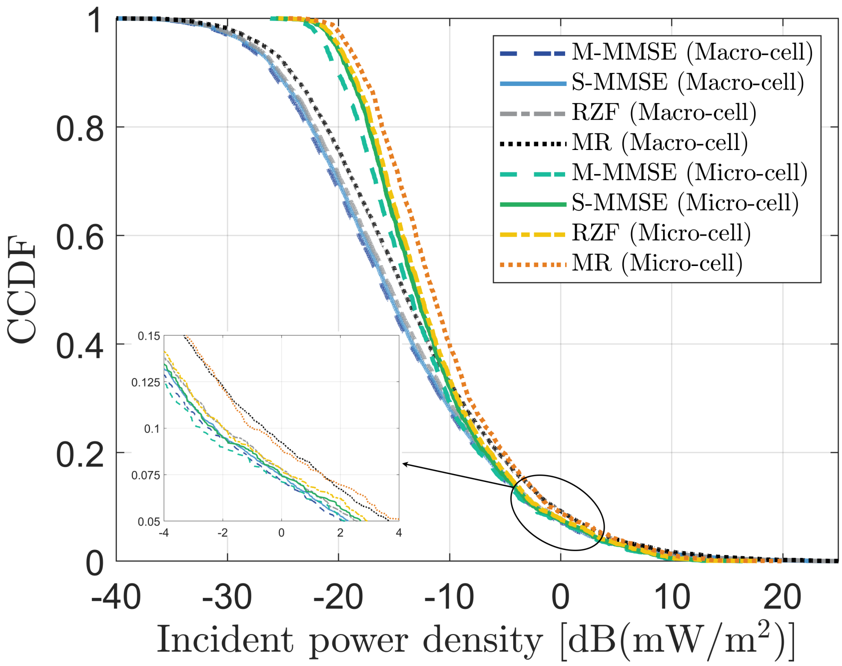

(a) Cellular

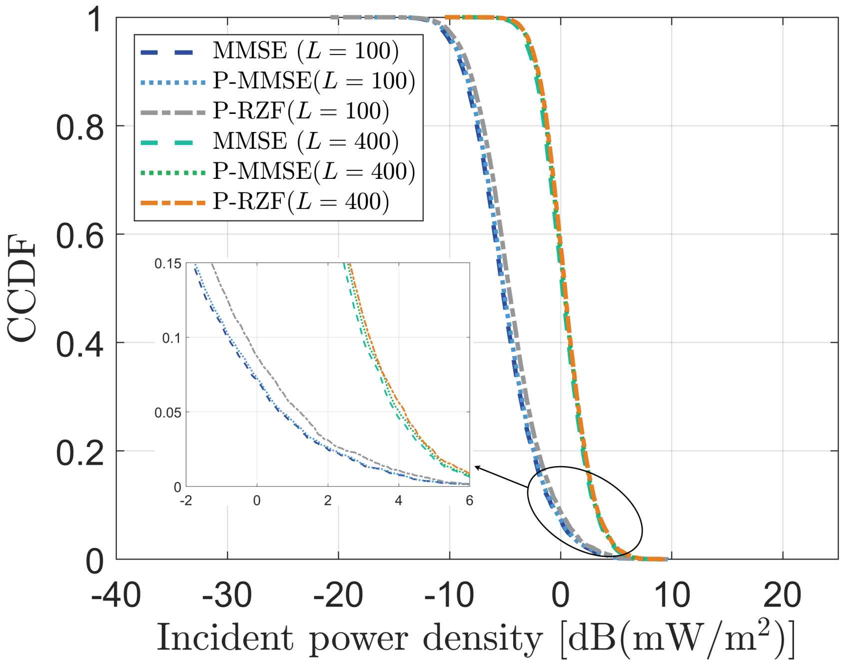

(b) Cell-free

Figure 5.4: CCDF of the incident power density in a cellular mMIMO network (a) and in a user-centric cell-free mMIMO network (b). Both simulations have been performed using perfect CSI on the UE side. The other parameters can be found in Table 5.1 for (a) and in Table 5.2 for (b).

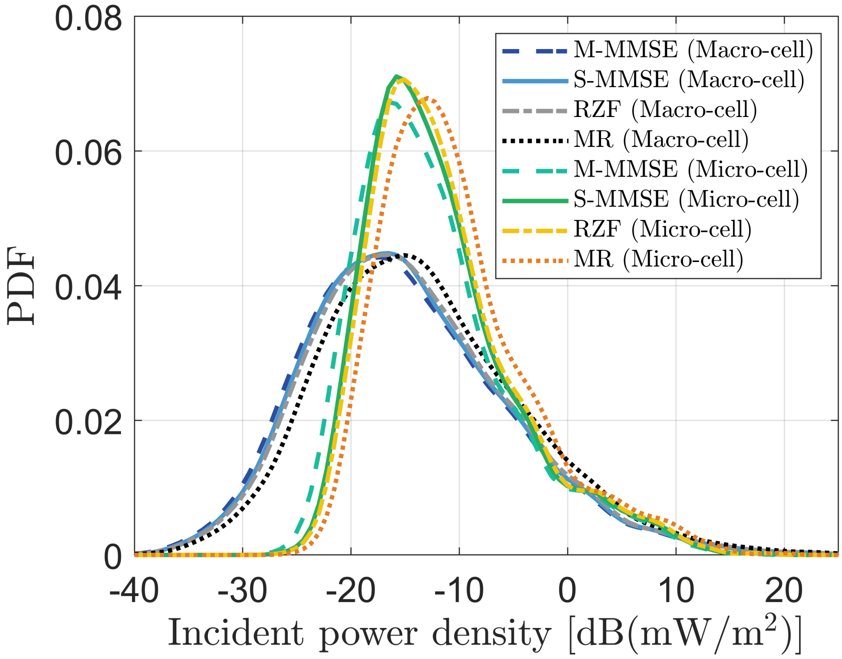

(a) Cellular

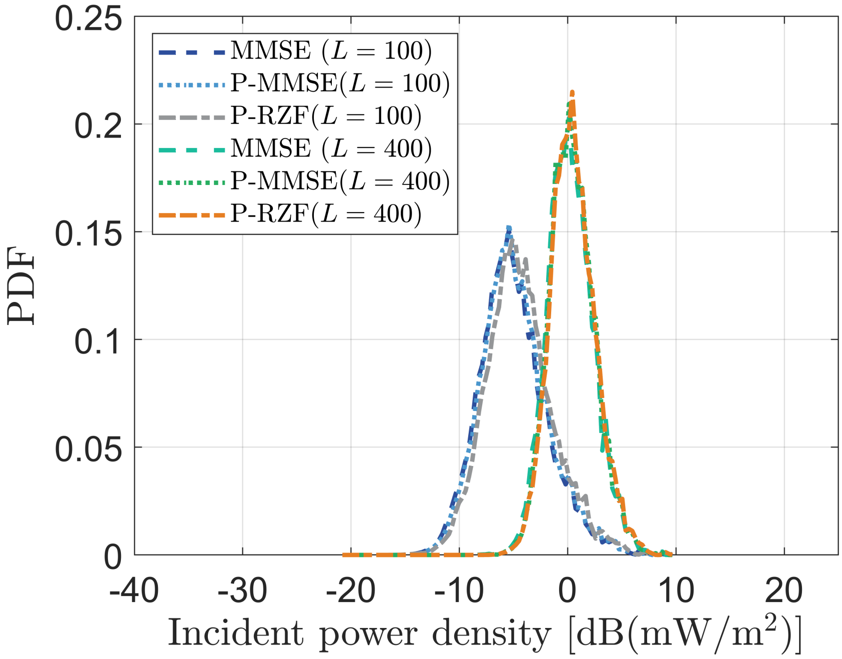

(b) Cell-free

Figure 5.5: PDF of the incident power density in a cellular mMIMO network (a) and in a user-centric cell-free mMIMO network (b). Both simulations have been performed using perfect CSI on the UE side. The other parameters can be found in Table 5.1 for (a) and in Table 5.2 for (b).

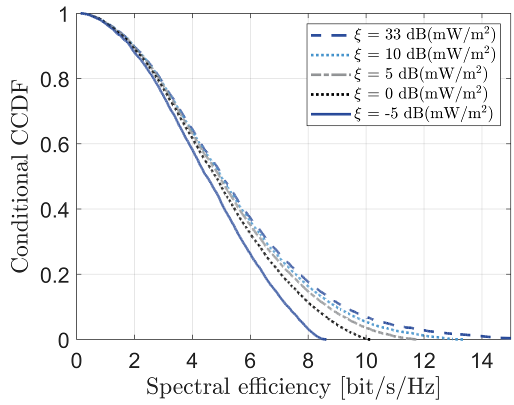

(a) Cellular conditional CCDF

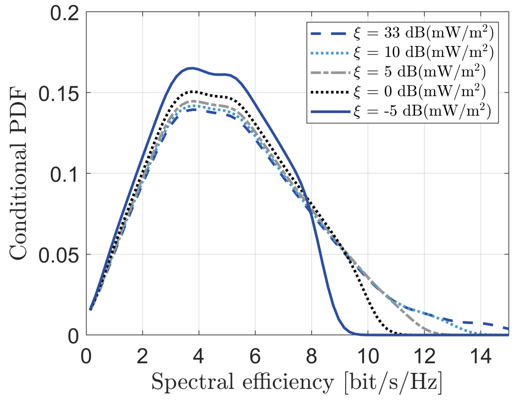

(b) Cellular conditional PDF

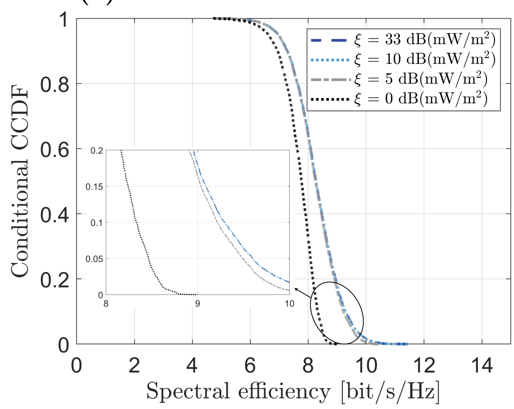

(c) Cell-free conditional CCDF

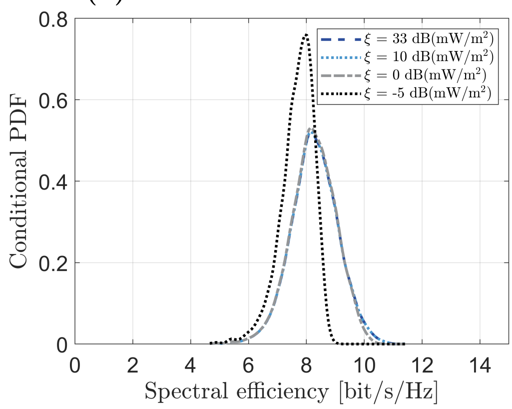

(d) Cell-free conditional PDF

Figure 5.6: Conditional CCDF $\bar{F}_{\mathrm{SE}|\xi}(T|T')$ and PDF of cellular network (a) and (b), using M-MMSE precoding and macro-cell channel model and cell-free network (c) and (d), using MMSE precoding with $L = 400$ and $N = 1$.

simulations) never reaches a value of $\xi = 33$ dB(mW/m^2). Consequently, restricting the SE according to the level of exposure only has an impact when the latter is really low. In cellular, however, some UEs may experience EMF exposure close to the limit set by the authorities. Therefore, limiting the exposure reduces the SE more quickly than in cell-free. Generally speaking, what these curves illustrate is that even if the average exposure is greater in cell-free than in cellular, the range of values that it can take in the first case is so limited that the room for manoeuvre that cell-free networks can take with respect to current limits is great.

Finally, the joint CCDF are illustrated in Figure 5.7. They provide the probability that SE $> T$ and $\xi \leq T'$. It shows the trad-offs that are made between the SE and the EMF exposure in the two types of networks.

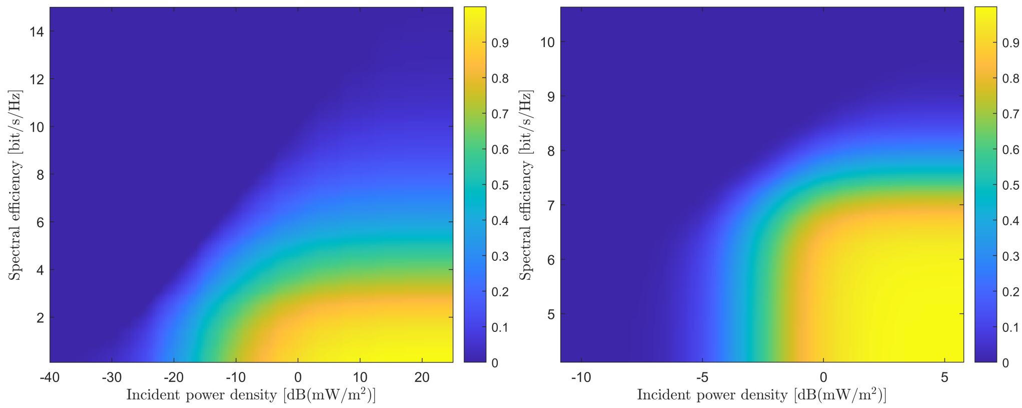

(a) Cellular **(b)** Cell-free

Figure 5.7: Joint CCDF $\bar{F}_{\mathrm{SE},\xi}(T, T')$ of cellular network (a), using M-MMSE precoding and macro-cell channel model and cell-free network (b), using MMSE precoding with $L = 400$ and $N = 1$.

5.1.4 Power Allocation Effects

As mentioned at the beginning of this chapter, the power allocation techniques vary from one type of network to another. In the initial cellular network simulations, 100 mW of power are allocated to each UE while in cell-free the sum of the powers allocated by each AP serving a UE k to that UE is equal on average to $\bar{\rho}_k = 102.06$ mW[4]. In order to compare them as well as possible, this section takes the performance of the cell-free setup where $L = 400$ and $N = 1$, defined in Table 5.2, and where the MMSE precoding scheme is used, as a reference model. This model is compared to the performance of a cellular network (using M-MMSE as precoding scheme[5]) where the average allocated power per UE can vary. For these setups, the cellular *Macro-cell* channel model described in Table 5.1 is used. The following power allocations are considered in Figures 5.8 and 5.9 :

1. The basic cellular setup described in Table 5.1. The allocated power per UE is equal to $\rho_{jk} = 100$ mW.
2. The basic cell-free setup described in Table 5.2. The average allocated power per UE is equal to $\bar{\rho}_{jk} = 102.06$ mW.
3. The same cell-free setup as described above but using a maximum downlink

[4]Since the allocated power per UE in cell-free is not a fixed value, it was relatively difficult to achieve on average 100 mW with precision. This is why there is a small difference between cellular and cell-free allocated power per UE

[5]MMSE in cell-free and M-MMSE in cellular have been selected because they offer the best performance in both networks.

transmit power per AP of 200 mW leading to an average allocated power per UE equal to 55.59 mW. Indeed, according to [3, 44, 45], 200 mW of maximum downlink power per AP seems to be a more realistic value than 400 mW. The latter has initially been used to remain consistent with the 100 mW allocated to each UE in the cellular network.

4. A cellular setup, similar to point 1., where each BS allocates 55.59 mW of power to every UE it serves in order to match with point 3.

5. A cellular setup each BS allocates enough power per UE served so that the average SE per UE is approximately equal to that of the setup in point 4. The amount of power per UE used in this case is equal to $\rho_{jk} = 500$ mW.

Figure 5.8 illustrates the CCDF (a) and PDF (b) of the SE for the different setups described above. Figure 5.9 does the same for the EMF exposure. The average values of the datasets used to illustrate these figures are summarized in Table 5.5. The average SE of cellular setup 5. is approximately the same as the one of the cell-free setup 4 (cf. Table 5.5). However, by looking at Figure 5.8, one can see that in fact 70% of the UEs still have a chance to experience better performance in the cell-free base model than in the cellular one. The average value is biased by the few high covered UEs of the cellular network. In addition, a huge amount of power was required to achieve such a value in the cellular network, which seems unrealistic.

The case where the total power consumption of the cellular network is the equal to $\rho_{jk} = 55.59$ mW (and the total power consumption of both networks is $\sum^{K} \rho_k \approx$ 2220 mW) gives the poorest performance in term of SE but, logically, also the lowest exposure as illustrated in Figure 5.9.

One can note in Table 5.5 that when the average power per UE grows from 55.59 mW to 100 mW, cellular networks gain on average 13.28% of SE while cell-free networks gain 9.32%. The exposure increases, for its part, proportionally to the power.

According to these simulations, as well as offering more consistent performance in terms of coverage, cell-free networks could also be more energy-efficient. Indeed achieving the same average SE in cellular networks requires a higher total network power consumption than in cell-free networks. In other words, the energy efficiency of both networks can be calculated as follows [36]:

$$\mathrm{EE} = \frac{\mathrm{SE}}{\sum\limits_{k=1}^{K} \rho_k} \tag{5.8}$$

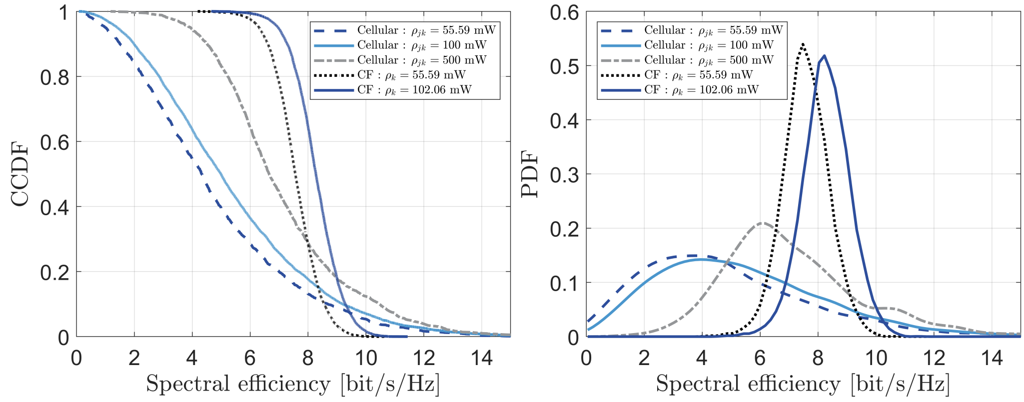

(a) **(b)**

Figure 5.8: CCDF (a) and PDF (b) of the SE of a cellular network and a cell-free network using different downlink allocated powers.

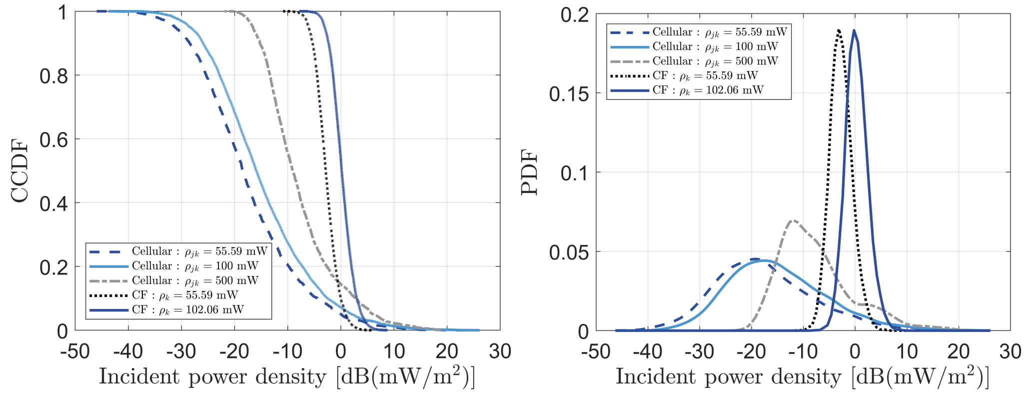

(a) **(b)**

Figure 5.9: CCDF (a) and PDF (b) of the EMF exposure of a cellular network and a cell-free network using different downlink allocated powers per UE.

Label	**Average SE [bits/s/Hz]**	**Average exposure [dB(mW/m^2)]**	**Average exposure [mW/m^2]**
Cellular : $\rho_{jk} = 55.59$ mW	4.750	-17.373	1.831×10^{-2}
Cellular : $\rho_{jk} = 100$ mW	5.381	-14.641	3.435×10^{-2}
Cellular : $\rho_{jk} = 500$ mW	7.384	-7.642	1.721×10^{-1}
CF : $\rho_k = 55.59$ mW	7.571	-2.739	5.323×10^{-1}
CF : $\rho_k = 102.06$ mW	8.277	0.270	1.065

Table 5.5: Average values of SE and EMF exposure for several downlink allocated power in cellular and cell-free networks

with the numerator being the average spectral efficiency and the denominator, the total power consumed by the network. This gives

$$\mathrm{EE}^{\mathrm{Cellular}} = 1.35 \times 10^{-3} \qquad\qquad \mathrm{EE}^{\mathrm{CF}} = 2.027 \times 10^{-3} \quad \frac{\mathrm{bit/s/Hz}}{\mathrm{W}} \tag{5.9}$$

5.1.5 Meta Distribution

Until now, the coverage metric was the spectral efficiency, who, as indicated in (3.19) for cellular networks and in (4.27) for cell-free networks, is an average over a large number of channel realizations. This results in an averaging of the small-scale fading effects. The large-scale fading, i.e. pathloss and shadowing, was considered as constant through all channel realizations since UEs are not moving. The meta distributions given in (5.6) for the SINR and in (5.7) for the EMF exposure are illustrated respectively in Figures 5.10 and 5.11. These figures provide the percentage of UEs experiencing at least a given SINR T (resp. EMF exposure T') during a certain percentage of the time given a position in the network. The instantaneous SINR is used instead of the SE here since the time dimension is now introduced and therefore the statistics cannot be averaged through it anymore. These figures have been generated by randomly moving a UE $K_{\mathcal{F}}$ times through the network. For each position, $N_{\mathcal{F}}$ new channel realizations have been generated and the $N_{\mathcal{F}}$ values of associated SINR and EMF exposure were computed. From this, the probability that $x\%$ of the UEs experience a larger SINR (resp. a smaller EMF exposure) than a given treshold T (resp. T') for $s\%$ of the time can be computed.

Figures 5.10 depicts the fact that in cellular networks, the time does not have a significant impact on the coverage (considering that UEs are stationary during the period studied). This is represented by the *flatter* nature of the curves in Figure 5.10a. The SINR is mainly influenced by the large-scale fading. In cell-free however, the range of average values that the SINR can take is much more limited (the coverage is almost independent of the position of the UE) and therefore the impact of the small-scale fading is more visible on the meta distribution. It should be borne in mind, however, that these variations only represent a few tenths of a dB or even a few dB at most. Figure 5.11 illustrates the fact that the small-scale fading has, logically, no impact on the EMF exposure.

In fact, the meta distribution curves are flat because the values that SINR in cellular networks and exposure in both (this is not the case in Figure 5.10b) can, for different UEs, often vary significantly from the thresholds T set to generate these curves. A toy example of this situation is illustrated in Figure 5.12. By considering that the black line is one of the threshold chosen in the meta distribution figures, it

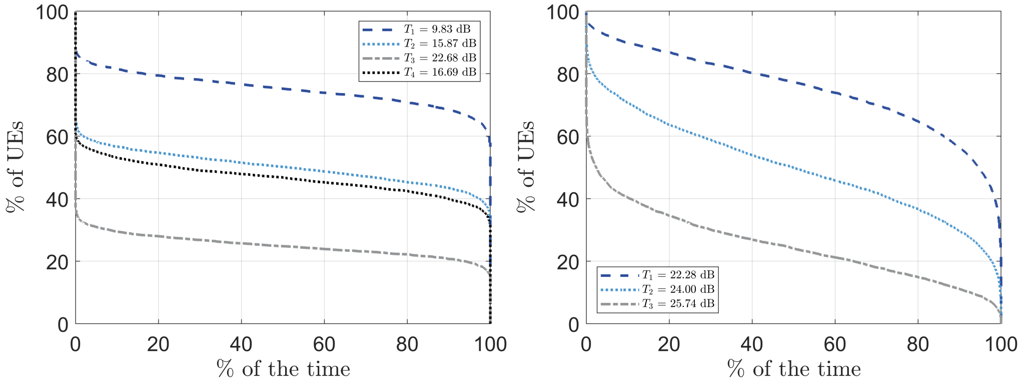

(a) Cellular **(b)** Cell-free

Figure 5.10: Meta distribution $\mathcal{F}_{\text{SINR}}(s,T)$ of the SINR [dB] for different thresholds T ($T_1, ..., T_4$ are respectively the first, second and third quartile and the mean of the SINR, except in (b) where Q_2 is equal to the mean).

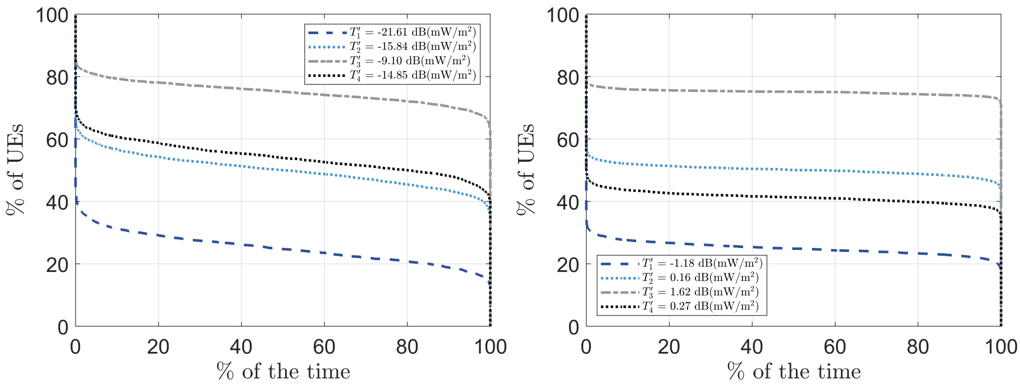

(a) Cellular **(b)** Cell-free

Figure 5.11: Meta distribution $\mathcal{F}_{\xi}(s,T)$ of the EMF exposure [dB(mW/m^2)] for different thresholds T' ($T'_1, ..., T'_4$ are respectively the first, second and third quartile and the mean of the EMF exposure).

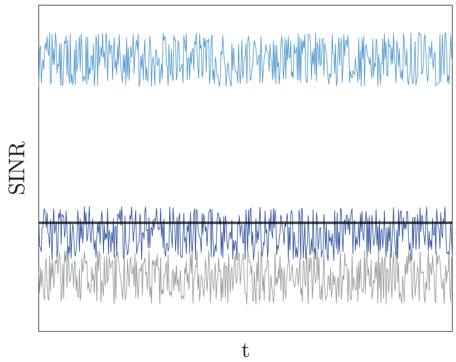

Figure 5.12: Fictive evolution of SINR over time in relation to a given threshold (the black line) for three stationary UEs in a communication network.

appears that only a few UE have a SINR represented in dark blue. In that case the average value of the SINR over time is close to T. Therefore the small-scale fading has an impact on the probability of exceeding or not exceeding this threshold. Most of them have SINR that never crosses the threshold. The average value is so far from the threshold that, even with the variations induced by the small-scale fading, it is either above (light blue curve) or below (gray curve) for any channel realization, making the meta distribution curves *flat*. The large-scale fading (which defines the average value of SINR and exposure) dominates the effects of the small-scale fading.

6

Performance Comparison of Cell-Free Networks for Three Pilot Assignement Schemes

Enhancing performance of cell-free systems can be achieved through a well-designed pilot assignment by mitigating the interference coming from the pilot-sharing UEs. In this section, the performance of three pilot assignement schemes are compared in term of SE. Their impact on the UEs EMF exposure is also discussed. In this chapter, the discussions focus solely on comparison between cell-free networks, and no longer with cellular networks.

6.1 Pilot Assignment Schemes Description

This section defines three scalable pilot assignement schemes that can be used in cell-free networks. The first one comes from the literature while the second one is a benchmark and the last one have been developed in the context of this document.

6.1.1 Joint AP Selection and Pilot Assignement

In the joint AP selection and pilot assignement scheme, described in Algorithm 2, the τ_p firstly dropped UEs in the network are assigned to orthogonal pilots $\{t_k = k : k = 1, ..., \tau_p\}$. The remaining $K - \tau_p$ UEs are assigned to a pilot according to the quality of their channel with a particular AP called *Master AP*. Indeed each

UE $k = \tau_p + 1, ..., K$ elects its master AP by taking the AP ℓ to which it has the strongest channel

$$\ell = \arg \max_{l \in \{1,...,L\}} \beta_{kl} \tag{6.1}$$

The designated master AP will browse every pilot t and find the index of the pilot who offers the least pilot contamination to its particular UE k and attributes it to him.

$$\tau = \arg \min_{t \in \{1,...,\tau_p\}} \sum_{\substack{i=1 \\ t_i = t}}^{k-1} \beta_{i\ell} \tag{6.2}$$

Once done, the algorithm restarts with the next UE.

Algorithm 2 Joint AP selection and pilot assignement

for $k = 1, ..., \tau_p$ **do**
  $\tau_p \leftarrow k$;
end for
for $k = \tau_p + 1, ..., K$ **do**
  $\ell \leftarrow \arg \max_{l \in \{1,...,L\}} \beta_{kl}$;
  $\tau \leftarrow \arg \min_{t \in \{1,...,\tau_p\}} \sum_{\substack{i=1 \\ t_i = t}}^{k-1} \beta_{i\ell}$;
  $t_k \leftarrow \tau$; ▷ As explained in Section 4.1.4, t_k is the pilot index of UE k
end for
Output: Pilot assignement $t_1, ..., t_K$;

This is a scalable algorithm. It has been proposed in [46]. Its goal is to be used jointly with the DCC technique defined in Algorithm 1.

6.1.2 Random Pilot Assignement

When the pilot sequences are assigned according to the random pilot assignement scheme, each UE gets a random pilot index $t_k = \text{randint}(1, \tau_p)$ going from 1 to τ_p (τ_p being the number of orthogonal pilot sequences) as described in Algorithm 3. In the simulation, UEs keep their pilot index over all coherence blocks.

This scheme is trivial to implement in practice, but faces two major problems. Firstly, there is no limit on the number of UEs assigned to each pilot. There

Algorithm 3 Random pilot assignement

1: **for** $k = 1, ..., K$ **do**
2: $\quad t_k \leftarrow \text{randint}(1, \tau_p)$;
3: **end for**
4: **Output:** Pilot assignement $t_1, ..., t_K$

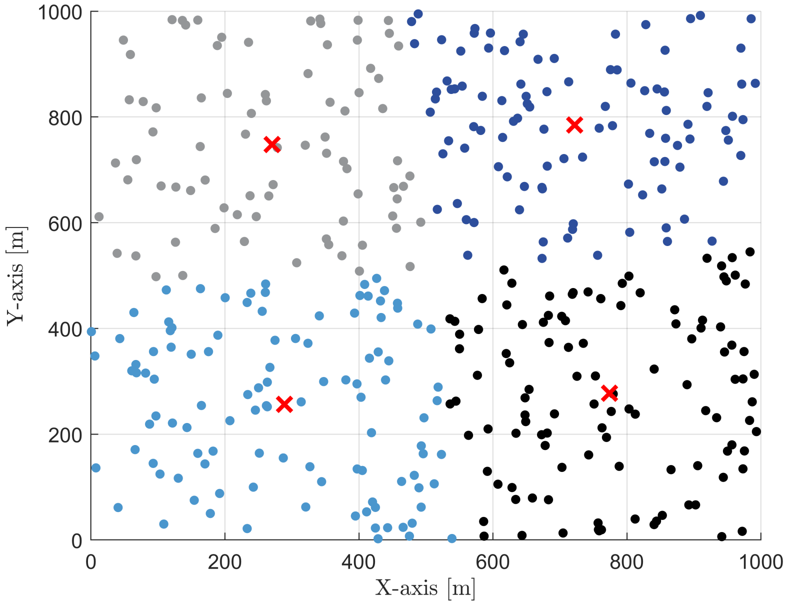

Figure 6.1: Example of K-Mean clustering (with $\lceil K/\tau_p \rceil = 4$) of APs in a randomly generated network ($L = 400$).

is therefore a chance that a certain pilot index will be assigned to a lot of UEs (whereas in the other two schemes, each pilot is assigned to $\lceil K/\tau_p \rceil$ UEs). These many pilot sharing UEs thus have a higher chance to experience pilot contamination. In addition, when two UEs are located closely, they may occasionally be assigned to the same pilot, leading to significant mutual interference.

6.1.3 K-Means Pilot Assignement

The K-Means pilot assignement scheme is geography-based since it divide the network into $\lceil K/\tau_p \rceil$ clusters using APs position, as illustrated in Figure 6.1. Thereafter, it allocates a cluster to each UE based on their distances with the different centroids (i.e. "centers" of the clusters). A maximum of τ_p UEs can be assigned to each centroid.

The proposed K-Means pilot assignement scheme works as follows

1. Randomly drop $\lceil K/\tau_p \rceil$ centroids in the network. Their positions are denoted $\mathbf{c}_m : m = 1, ..., \lceil K/\tau_p \rceil$. $\mathcal{C}_m$ and $\mathcal{C}'_m$ are respectively the set of APs and the set of UEs assigned to centroid m. They are both initialized to $\{\mathcal{C}_m, \mathcal{C}'_m = \emptyset : m = 1, ..., \lceil K/\tau_p \rceil\}$. $\mathbf{x}_l^{\text{AP}}$ and $\mathbf{x}_k^{\text{UE}}$ denote respectively the coordinates of AP l and of UE k in the network area. $\mathcal{L}_{\text{UE}}$ is the set of UEs who have not yet been allocated a pilot. Initially, it contains the index of all the UEs.

2. The K-Means clustering phase extends from steps [2-11] in Algorithm 4. Every AP is assigned to its closest centroid and than the position of each centroid is updated, taking into account the average position of all APs allocated to them. This is repeated until the convergence is reached. In this case, convergence means that the change in position of each centroid between the last two iterations is less than a certain threshold ϵ (in this case $\epsilon = 0.01$ m). In other cases, convergence can simply be a fixed number of iterations.

3. When the clusters are formed, each UE is assigned to its closest centroid one by one. If a new UE is assigned to cluster m whose $|\mathcal{C}'_m| < \tau_p$, there is no issue (since the maximum number of UEs assigned to this cluster is not reached yet) and the index of this UE is removed from $\mathcal{L}_{\text{UE}}$. However, when $|\mathcal{C}'_m| = \tau_p$, a competition is initiated. The new UE compares its distance to the centroid with the UE already assigned to this centroid who has the greatest distance. If the new UE is closer, it takes the place of the already assigned UE, which is returned to the set $\mathcal{L}_{\text{UE}}$. If he is not closer, the centroid m is blacklisted for this UE which stays in the set $\mathcal{L}_{\text{UE}}$ and the algorithm starts again.

4. Once all UEs have been assigned to a centroid, they receive a pilot index as described in steps [28-30]. The pilots of the UEs belonging to the same centroid are orthogonal.

The pseudocode is provided in Algorithm 4.

In some way, the K-Means pilot assignement divides the network into cells. Each pilot is only used once in a cell. The pilot assignement is however the only part of the network processing working in that way. The main advantage of this technique is that the clustering can be precomputed since it relies on the APs locations which are considered as fixed. By not taking the clustering into account when defining the complexity (since considered as precomputed) of the pilot assignement, it gives a complexity of $\mathcal{O}(K)$ (since τ_p is considered as constant in the network) which makes it a scalable scheme. K-Means pilot assignement also have drawbacks. Firstly, even if inside a cluster all the pilot are orthogonal, nothing prevents two closely located UEs, belonging to two different clusters, from sharing the same pilot. Secondly, a few UEs (i.e. UEs that are not assigned to their closest centroid) can be located relatively far from their assigned centroid due to the limit τ_p of assigned UEs per

Algorithm 4 K-Means pilot assignement

Initialization: Randomly drop $\lceil K/\tau_p \rceil$ centroids in the network area;
repeat
  $\mathcal{C}_m \leftarrow \emptyset, \forall m = 1, ..., \lceil K/\tau_p \rceil$;
  for $1 \leq l \leq L$ **do**
    $m^* = \arg\min_m \left|\left|\mathbf{c}_m - \mathbf{x}_l^{\mathrm{AP}}\right|\right|_2^2, \forall m = 1, ..., \lceil K/\tau_p \rceil$;
    $\mathcal{C}_{m^*} \leftarrow \mathcal{C}_{m^*} \cup \{l\}$;
  end for
  for $1 \leq m \leq \lceil K/\tau_p \rceil$ **do**
    $\mathbf{c}_m \leftarrow \frac{1}{|\mathcal{C}_m|} \sum_{l \in \mathcal{C}_m} \mathbf{x}_l$;
  end for
until Convergence
$\mathcal{C}'_m = \emptyset, \forall m = 1, ..., \lceil K/\tau_p \rceil$;
while $|\mathcal{L}_{\mathrm{UE}}| > 0$ **do**
  $m^* = \arg\min_m \left|\left|\mathbf{c}_m - \mathbf{x}_{\mathcal{L}_1}^{\mathrm{UE}}\right|\right|_2^2$; ▷ $\mathcal{L}_1$ is the first element of $\mathcal{L}_{\mathrm{UE}}$
  if $|\mathcal{C}'_{m^*}| < \tau_p$ **then**
    $\mathcal{C}'_{m^*} \leftarrow \mathcal{C}'_{m^*} \cup \{\mathcal{L}_1\}$;
    $\mathcal{L}_{\mathrm{UE}} \leftarrow \mathcal{L}_{\mathrm{UE}} / \{\mathcal{L}_1\}$;
  else
    $k^* = \arg\max_k \left|\left|\mathbf{c}_{m^*} - \mathbf{x}_k^{\mathrm{UE}}\right|\right|_2^2, \forall k \in \mathcal{C}'_{m^*}$;
    if $\left|\left|\mathbf{c}_{m^*} - \mathbf{x}_{\mathcal{L}_1}^{\mathrm{UE}}\right|\right|_2^2 < \left|\left|\mathbf{c}_{m^*} - \mathbf{x}_{k^*}^{\mathrm{UE}}\right|\right|_2^2$ **then**
      $\mathcal{C}'_{m^*} \leftarrow \mathcal{C}'_{m^*} / \{k^*\} \cup \{\mathcal{L}_1\}$;
      $\mathcal{L}_{\mathrm{UE}} \leftarrow \mathcal{L}_{\mathrm{UE}} / \{\mathcal{L}_1\} \cup \{k^*\}$;
    else
      $\left|\left|\mathbf{c}_{m^*} - \mathbf{x}_{\mathcal{L}_1}^{\mathrm{UE}}\right|\right|_2 \leftarrow \infty$; ▷ UE $\mathcal{L}_1$ blacklists the centroid m^* by setting the distance between them to ∞
    end if
  end if
end while
for $1 \leq i \leq \tau_p$ **do**
  $t_{\mathcal{C}_{m_i}} \leftarrow i, \forall m = 1, ..., \lceil K/\tau_p \rceil$; ▷ $\mathcal{C}_{m_i}$ is the ith element of the set $\mathcal{C}_m$
end for
Output: Pilot assignement $t_1, ..., t_K$

centroid. These UEs also have a chance of finding themselves close to pilot sharing UEs from other clusters and therefore experience pilot contamination. There exists many other pilot assignement algorithms, some of them are listed in [5, Table VI]. Most of them are however unscalable.

6.2 Numerical Performance Analysis

CCDF and PDF of the SE and EMF exposure experienced by UEs in a cell-free network using the three pilot assignement schemes described above are provided in Figure 6.2. As a first observation from Figure 6.2d, one can see that that the joint AP selection and pilot assignement outperforms the K-Means scheme, which offers better performance than the random scheme. This can be explained by the fact that in the first case, pilots are chosen based on the master AP that provides the best channel gain, while in the second case, the pilot depends solely on the UE's relative positions to centroids in the network. These pilot assignement provides approximately the same EMF exposure. In fact, it does not influence the power allocation and the number of APs serving each UEs does not change significantly.

This K-Means pilot assignement algorithm does not have any particular advantage compared to the joint AP selection and pilot assignement since it offers almost similar performance with the same computational complexity (indeed the complexity of this last is also $\mathcal{O}(K)$, when considering the pilot assignement without the DCC). It has, however, the advantage of being easier to compute than other clustering algorithms proposed in the literature as in [23, 47], while offering good performance. It could be interesting in other cases to build clusters based, not only on the positions of the APs but jointly considering the positions of the UEs and APs or making use of interference.

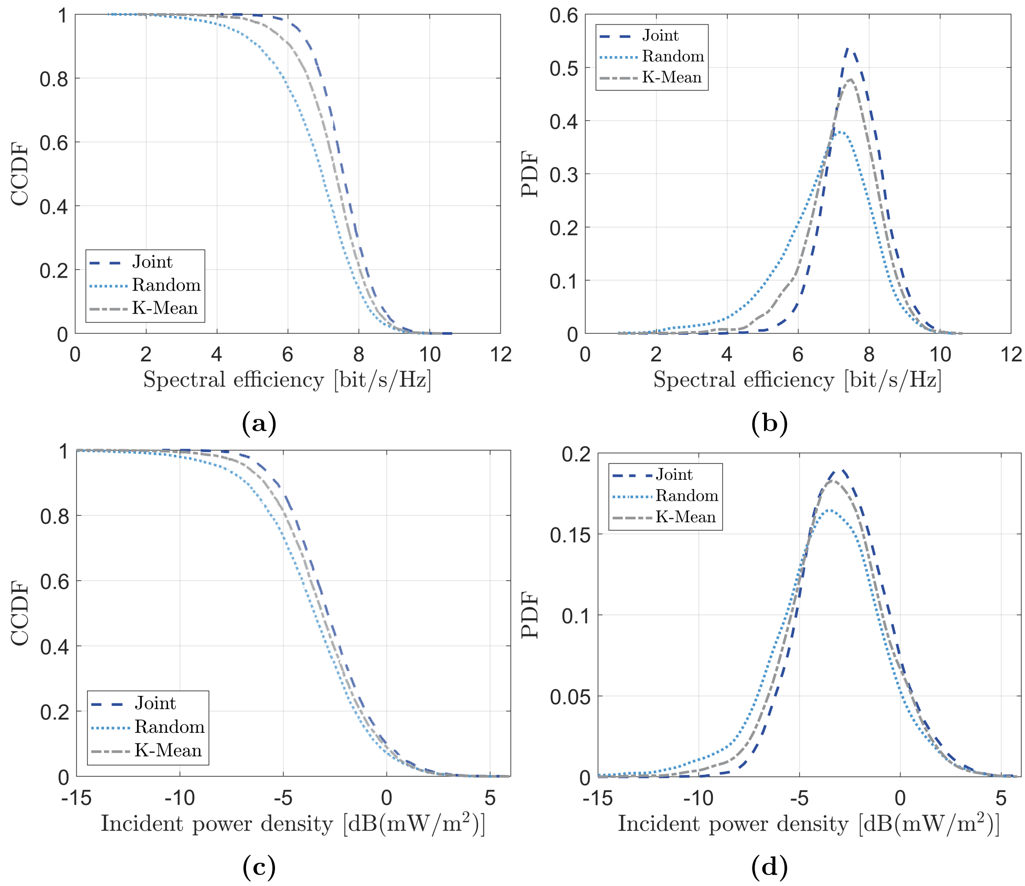

Figure 6.2: CCDF and PDF of the SE and EMF exposure in a cell-free network using three pilot assignement schemes.

7

Conclusion

The goal of this document was to provide a comparison of spectral efficiency and electromagnetic field (EMF) exposure levels achievable in cellular and cell-free massive MIMO networks. Performance of these networks were compared through numerical simulations, using several statistical metrics. The system models used in the simulations were defined in advance, as were the various metrics. It is important to bear in mind that certain simplifying assumptions (mentioned through the work) were used when simulating these networks. As this investigation is drawing to a close, several key insights have emerged.

Objectives and Key Findings

The primary aim was to assess whether cell-free networks could deliver, through massive MIMO configurations, a spectral efficiency at least comparable to that of traditional cellular networks while maintaining EMF exposure within acceptable limits. The simulations, conducted under simplified models featuring 400 antennas and 40 UEs, revealed nuanced outcomes.

- **Spectral efficiency analysis:** On average, cell-free networks demonstrated a superior spectral efficiency compared to their cellular counterparts. The cooperative serving clusters of spatially distributed transmitters in cell-free architectures showed the ability to enhance spectral efficiency and above all in a much more uniform way than cellular networks. However, it's noteworthy that maximum achievable spectral efficiency values should still be provided by cellular networks. This suggests that while cell-free networks have the potential to improve average performance, specific scenarios might favor the traditional cellular setup.

- **EMF exposure evaluation:** On average, a higher level of exposure in cell-free networks compared to cellular networks is observed. This is because the proximity UEs have with their serving APs results in relatively low attenuation of exposure power. In contrast, cellular networks exhibit a more varied distance between UEs and BSs, contributing to a lower average exposure. In cell-free networks, the exposure levels display minimal variability from one UE to another. Consequently, the maximum exposure closely aligns with the average value, reflecting a more uniform distribution of EMF exposure. This predictability is a notable advantage in managing and regulating exposure levels within the network. Conversely, cellular networks exhibit a more diverse exposure profile. While the average exposure is lower than that in cell-free networks, the range of exposure values is considerably wider, indicating a higher variance. This results in a maximum exposure value that deviates significantly from the average, surpassing even the maximum exposure observed in cell-free networks.

Cell-free networks, given their cooperative and spatially distributed nature, hold promise for enhancing spectral efficiency while simultaneously managing EMF exposure within a relatively confined range of values. However, the results underscore the importance of carefully considering the trade-offs, particularly in scenarios where maximum performance is critical. Furthermore, cell-free networks exhibit great potential for effectively serving the communication needs of densely populated urban areas, where the strategic deployment of numerous APs is logistically feasible. However, the scalability and practicality of deploying a multitude of APs per square kilometer may pose challenges in rural or less densely populated areas. The deployment of cell-free networks, therefore, goes hand in hand with a global heterogenization of communication networks.

To refine and extend the work proposed here, here are a few suggestions.

1. Current simulations were based on simplified models, particularly in terms of cellular network topology. Exploring a broader range of scenarios using, for example, stochastic geometry in order to emulate the deployment of the BSs would provide a more nuanced perspective. Furthermore, a closer examination of the interactions between network size and UEs density could yield valuable insights.

2. In the current simulations for both network scenarios, power allocations are determined using heuristics. An avenue for enhancing the study would involve developing more realistic power allocation strategies. This could entail considering dynamic power control mechanisms or incorporating adaptive

algorithms that better emulate real-world scenarios. While maintaining the feasibility of comparison, these adjustments would contribute to a more accurate representation of the networks' behaviors under varying conditions, providing a nuanced perspective on their respective performances.

3. Define a rigorous downlink channel estimation for both types of networks to eliminate the assumption of UEs having perfect knowledge of the Channel State Information (CSI). This would provide a more realistic comparison. This could be done, for example, by means of a downlink pilot signal.

4. Improvements to the K-Means pilot assignement algorithm provided in Section 6.1.3 can be made by taking into account the distance between the UEs after the cluster assignement.

In conclusion, there is still a journey ahead to define cell-free networks as a practical application. However, with highly homogeneous coverage and exposure levels, they seem to be a solution capable of addressing the challenges that future generations of telecommunication networks will face.

Bibliography

[1] Samsung. *White Paper: The Vision of 6G Bring the Next Hyper-Connected Experience to Every Corner of Life.* https://research.samsung.com/next-generation-communications. 2020.

[2] Marco Giordani et al. "Toward 6G Networks: Use Cases and Technologies". In: *IEEE Communications Magazine* 58.3 (2020), pp. 55–61. DOI: 10.1109/MCOM.001.1900411.

[3] Özlem Tuğfe Demir, Emil Björnson, and Luca Sanguinetti. *Foundations of User-Centric Cell-Free Massive MIMO*. Now Publishers, 2021. DOI: https://www.nowpublishers.com/article/Details/SIG-109.

[4] Hussein A. Ammar et al. "User-centric Cell-free Massive MIMO Networks: A Survey of Opportunities, Challenges and Solutions". In: (Dec. 2021), pp. 611–652. DOI: 10.1109/COMST.2021.3135119.

[5] Shuaifei Chen et al. *A Survey on User-Centric Cell-Free Massive MIMO Systems*. 2021. arXiv: 2104.13667 [cs.IT].

[6] Ring D. H. "Mobile Telephony - Wide Area Coverage". In: *Bell Laboratories Technical Memorandum* (1947).

[7] R.H. Frenkiel. "A high-capacity mobile radiotelephone system model using a coordinated small-zone approach". In: *IEEE Transactions on Vehicular Technology* 19.2 (1970), pp. 173–177. DOI: 10.1109/T-VT.1970.23447.

[8] W. R. Young. "Advanced mobile phone service: Introduction, background, and objectives". In: *The Bell System Technical Journal* 58.1 (1979), pp. 1–14. DOI: 10.1002/j.1538-7305.1979.tb02208.x.

[9] Emil Björnson, Jakob Hoydis, and Luca Sanguinetti. *Massive MIMO Networks: Spectral, Energy, and Hardware Efficiency*. 2017.

[10] Ericsson. *Ericsson mobility report*. https://www.ericsson.com/en/reports-and-papers/mobility-report. 2023.

[11] Nusrat Fatema et al. "Massive MIMO Linear Precoding: A Survey". In: *IEEE Systems Journal* 12.4 (2018), pp. 3920–3931. DOI: 10.1109/JSYST.2017.2776401.

[12] Hong Yang and Thomas L. Marzetta. "Performance of Conjugate and Zero-Forcing Beamforming in Large-Scale Antenna Systems". In: *IEEE Journal on Selected Areas in Communications* 31.2 (2013), pp. 172–179. DOI: 10.1109/JSAC.2013.130206.

[13] V. H. Mac Donald. "Advanced mobile phone service: The cellular concept". In: *The Bell System Technical Journal* 58.1 (1979), pp. 15–41. DOI: 10.1002/j.1538-7305.1979.tb02209.x.

[14] Thomas L. Marzetta. "Fundamentals of Massive MIMO". In: *Cambridge University Press* (2016). DOI: https://doi.org/10.1017/CBO9781316799895.

[15] Thomas L. Marzetta. "Noncooperative Cellular Wireless with Unlimited Numbers of Base Station Antennas". In: *IEEE Transactions on Wireless Communications* 9.11 (2010), pp. 3590–3600. DOI: 10.1109/TWC.2010.092810.091092.

[16] Pang Xingdong et al. "Design and implementation of an active multibeam antenna system with 64 RF channels and 256 antenna elements for massive MIMO application in 5G wireless communications". In: *China Communications* 11.11 (2014), pp. 16–23. DOI: 10.1109/CC.2014.7004520.

[17] Fredrik Rusek et al. "Scaling Up MIMO: Opportunities and Challenges with Very Large Arrays". In: *IEEE Signal Processing Magazine* 30.1 (2013), pp. 40–60. DOI: 10.1109/MSP.2011.2178495.

[18] Jeffrey G. Andrews et al. "Are we approaching the fundamental limits of wireless network densification?" In: *IEEE Communications Magazine* 54.10 (2016), pp. 184–190. DOI: 10.1109/MCOM.2016.7588290.

[19] Jun Wu et al. "Cloud radio access network (C-RAN): a primer". In: *IEEE Network* 29.1 (2015), pp. 35–41. DOI: 10.1109/MNET.2015.7018201.

[20] Hien Quoc Ngo et al. "Cell-Free Massive MIMO: Uniformly great service for everyone". In: *2015 IEEE 16th International Workshop on Signal Processing Advances in Wireless Communications (SPAWC)*. 2015, pp. 201–205. DOI: 10.1109/SPAWC.2015.7227028.

[21] Stefano Buzzi and Carmen D'Andrea. "User-Centric Communications versus Cell-free Massive MIMO for 5G Cellular Networks". In: *WSA 2017; 21th International ITG Workshop on Smart Antennas*. 2017, pp. 1–6.

[22] Jiayi Zhang et al. "Cell-Free Massive MIMO: A New Next-Generation Paradigm". In: *IEEE Access* 7 (2019), pp. 99878–99888. DOI: 10.1109/ACCESS.2019.2930208.

[23] Shuaifei Chen et al. "Structured Massive Access for Scalable Cell-Free Massive MIMO Systems". In: *IEEE Journal on Selected Areas in Communications* 39.4 (2021), pp. 1086–1100. DOI: 10.1109/JSAC.2020.3018836.

[24] Giovanni Interdonato et al. "Ubiquitous cell-free Massive MIMO communications". In: *EURASIP Journal on Wireless Communications and Networking* 2019.1 (Aug. 2019). ISSN: 1687-1499. DOI: 10.1186/s13638-019-1507-0. URL: http://dx.doi.org/10.1186/s13638-019-1507-0.

[25] Salah Elhoushy, Mohamed Ibrahim, and Walaa Hamouda. "Cell-Free Massive MIMO: A Survey". In: *IEEE Communications surveys & Tutorials* (2022), pp. 492–523. DOI: https://ieeexplore.ieee.org/stamp/stamp.jsp?tp=&arnumber=9586055&tag=1.

[26] L. El Amrani, T. Mazri, and N. Hmina. "The Specific Absorption Rate induced in human organs due Ionizing and Non Ionizing Radiations exposure". In: *2018 6th International Conference on Wireless Networks and Mobile Communications (WINCOM)*. 2018, pp. 1–4. DOI: 10.1109/WINCOM.2018.8629631.

[27] *Centers for Disease Control and Prevention : Radiation and Your Health*. https://www.cdc.gov/. Accessed: 05-12-2023.

[28] Richard A. Tell. "Broadcast radiation: how safe is safe?" In: *IEEE Spectrum* 9.8 (1972), pp. 43–51. DOI: 10.1109/MSPEC.1972.5219017.

[29] Caroline Rodgers. "Dental X-ray exposure and Alzheimer's disease: A hypothetical etiological association". In: *Medical hypotheses* 77 (Mar. 2011), pp. 29–34. DOI: 10.1016/j.mehy.2011.03.016.

[30] Luca Chiaraviglio, Ahmed Elzanaty, and Mohamed-Slim Alouini. "Health Risks Associated With 5G Exposure: A View From the Communications Engineering Perspective". In: *IEEE Open Journal of the Communications Society* 2 (2021), pp. 2131–2179. DOI: 10.1109/OJCOMS.2021.3106052.

[31] Daniele Franci et al. "Experimental Procedure for Fifth Generation (5G) Electromagnetic Field (EMF) Measurement and Maximum Power Extrapolation for Human Exposure Assessment". In: *Environments* 7.3 (2020). ISSN: 2076-3298. DOI: 10.3390/environments7030022. URL: https://www.mdpi.com/2076-3298/7/3/22.

[32] Amina Fellan and Hans D. Schotten. “Overview of the Evaluation Methods for the Maximum EMF Exposure in 5G Networks”. In: *2022 IEEE Conference on Standards for Communications and Networking (CSCN)*. 2022, pp. 53–57. DOI: 10.1109/CSCN57023.2022.10050915.

[33] International Commission on Non-Ionizing Radiation Protection. *ICNIRP guidelines on limiting the exposure to time-varying electric, magnetic, and electromagnetic fields (100 kHz to 300 GHz)*. Vol. 118. Health Phys 5. 2020, pp. 483–524.

[34] Joumana Kassam et al. “A Review on Cell-Free Massive MIMO Systems”. In: *Electronics* 12.4 (2023). ISSN: 2079-9292. DOI: 10.3390/electronics12041001. URL: https://www.mdpi.com/2079-9292/12/4/1001.

[35] *5G et santé*. https://parlons5g.be/theme/sante. Accessed: 05-12-2023.

[36] Charles Wiame. “Joint coverage and EMF exposure analysis in cellular and cell-free networks : a stochastic geometry perspective”. In: (2023). DOI: http://hdl.handle.net/2078.1/277418.

[37] Joao Vieira et al. “Reciprocity Calibration for Massive MIMO: Proposal, Modeling, and Validation”. In: *IEEE Transactions on Wireless Communications* 16.5 (2017), pp. 3042–3056. DOI: 10.1109/TWC.2017.2674659.

[38] Henrik Asplund, Kjell Larsson, and Peter Okvist. “How Typical is the Typical Urban channel model?” In: June 2008, pp. 340–343. ISBN: 978-1-4244-1644-8. DOI: 10.1109/VETECS.2008.82.

[39] Elina Nayebi et al. “Precoding and Power Optimization in Cell-Free Massive MIMO Systems”. In: *IEEE Transactions on Wireless Communications* 16.7 (2017), pp. 4445–4459. DOI: 10.1109/TWC.2017.2698449.

[40] Hien Quoc Ngo et al. “Cell-Free Massive MIMO Versus Small Cells”. In: *IEEE Transactions on Wireless Communications* 16.3 (2017), pp. 1834–1850. DOI: 10.1109/TWC.2017.2655515.

[41] Luca Sanguinetti, Emil Björnson, and Jakob Hoydis. “Toward Massive MIMO 2.0: Understanding Spatial Correlation, Interference Suppression, and Pilot Contamination”. In: *IEEE Transactions on Communications* 68.1 (2020), pp. 232–257. DOI: 10.1109/TCOMM.2019.2945792.

[42] 3GPP. *Further advancements for E-UTRA physical layer aspects (Release 9)*. 3GPP TS 36.814. 2017.

[43] 3GPP. *Further advancements for E-UTRA physical layer aspects (Release 9)*. 3GPP TS 36.814. 2010.

[44] Arezoo Izadi, S. Mohammad Razavizadeh, and O. Saatlou. “Power Allocation for Downlink Training in Cell-Free Massive MIMO Networks”. In: *2020 10th International Symposium onTelecommunications (IST)*. 2020, pp. 111–115. DOI: 10.1109/IST50524.2020.9345873.

[45] Mohamed Elwekeil, Alessio Zappone, and Stefano Buzzi. “Optimal Joint Beamforming and Power Control in Cell-Free Massive MIMO Downlink”. In: *2021 IEEE 22nd International Workshop on Signal Processing Advances in Wireless Communications (SPAWC)*. 2021, pp. 81–85. DOI: 10.1109/SPAWC51858.2021.9593141.

[46] Emil Björnson and Luca Sanguinetti. “Scalable Cell-Free Massive MIMO Systems”. In: *IEEE Transactions on Communications* 68.7 (2020), pp. 4247–4261. DOI: 10.1109/TCOMM.2020.2987311.

[47] Masoud Attarifar, Aliazam Abbasfar, and Angel Lozano. “Random vs Structured Pilot Assignment in Cell-Free Massive MIMO Wireless Networks”. In: *2018 IEEE International Conference on Communications Workshops (ICC Workshops)*. 2018, pp. 1–6. DOI: 10.1109/ICCW.2018.8403508.

UNIVERSITÉ CATHOLIQUE DE LOUVAIN
École polytechnique de Louvain
Rue Archimède, 1 bte L6.11.01, 1348 Louvain-la-Neuve, Belgique | **www.uclouvain.be/epl**